UNIVERSITI
MALAYSIA
KELANTAN

Effect of Adding Sawdust on Physical and Mechanical Properties in Ceramic Bricks

Sakthy Thevi A/P Pakianatan
J20G0754

A thesis submitted in fulfilment of the requirements for the degree of Bachelor of Applied Science (Materials Technology) with Honours

FACULTY OF BIOENGINEERING AND TECHNOLOGY
UMK

2024

DECLARATION

I declare that this thesis entitled "Effect of Adding Sawdust on Physical and Mechanical Properties in Ceramic Bricks" is the result of my own research except as cited in the references.

Signature : _____

Student's Name : SAKTHY THEVI A/P PAKIANATAN

Date : _____

Verified by:

Signature : _____

Supervisor's Name : DR. NORFADHILAH BINTI IBRAHIM

Stamp : _____

Date : _____

ACKNOWLEDGEMENT

First and foremost, I sincerely thank my supervisor, Dr. Norfadhilah Binti Ibrahim, for her unwavering support throughout my study and research for my Final Year Project (FYP). I am grateful for her patience, motivation, guidance, and extensive knowledge. Furthermore, I am thankful for her unwavering support and encouragement throughout this Final Year Project, which ultimately led to its completion. Despite her demanding schedule filled with work and meetings, she consistently made time to guide me to complete my FYP efficiently.

Furthermore, I would like to thank the laboratory assistants at UMK for their valuable support in operating diverse characterization equipment and conducting laboratory procedures. I thank the lab assistants, Mrs Hanisah, Mrs Syahirah, Mrs Ayu, Mr Qamal, and Mr Afifi, for guiding me through the tests conducted during my FYP days. I would like to express my heartfelt appreciation to the remaining members of my final year project team for collectively collaborating and overcoming these challenges until we achieved successful completion.

Finally, I want to convey my appreciation to my family and friends who put their belief in me through their encouragement and support throughout this Final Year Project. I wish to express my gratitude to all those who aided me in completing my Final Year Project, whether directly or indirectly, and acknowledge my perseverance in persisting until the end of this endeavour. Those experiences will endure indefinitely.

Kesan Penambahan Habuk Papan pada Sifat Fizikal dan Mekanikal dalam Bata Seramik

ABSTRAK

Dalam kajian ini, kesan penambahan serbuk kayu pada sifat fizikal dan mekanikal telah disiasat. Tanah liat bola dan kaolin yang digabungkan dengan 0, 2.5, 4, 8 dan 10 wt.% daripada serbuk kayu telah diuji. Sampel batu bata seramik terbakar pada 900 °C,1000 °C dan 1100 °C serta sifat-sifatnya telah disiasat menggunakan XRD, FTIR, TGA, kepadatan, keliangan, penyerapan air dan ujian kekuatan mampatan. Kehadiran kuarza, mullite, moscovite dan kaolinite diyakini meningkatkan sifat-sifat batu bata keramik. Hasil analisis FTIR menunjukkan bahawa pengikat Si-O yang merupakan sebatian silika yang terbentuk dalam batu bata keramik diyakini mewujudkan rangkaian yang memberikan kekuatan dan kekakuan kepada matriks keramik. Hasil TGA menunjukkan kehilangan berat sampel dan sifat termal batu bata Keramik. Hasil percubaan menunjukkan bahawa penggunaan serbuk kayu mengurangkan kepadatan dan kekuatan kompresif sampel. Ia diamati pada poros yang kelihatan di mana dengan peningkatan serbuk kayu hingga 10 wt.%, poros kelihatan meningkat sehingga 40 % selepas pembakaran pada 900 °C. Kekuatan kompresif batu bata keramik dengan 2.5 wt.% serbuk kayu dan pembakaran pada 1100 °C menunjukkan nilai kekuatan yang lebih tinggi. Penyerapan air juga meningkat dengan peningkatan penambahan serbuk kayu sehingga 10 wt. %. Hasil-hasil itu menunjukkan bahawa penambahan sisa serbuk-serbuk mungkin bahan untuk ditambahkan kepada batu bata tanah liat mentah untuk menghasilkan sebagai seramik poros dan ringan.

Kata Kunci: Seramik batu bata, Serbuk kayu, Suhu pembakaran, Ciri-ciri fizikal, Sifat mekanikal

Effect of Adding Sawdust on Physical and Mechanical Properties in Ceramic Bricks

ABSTRACT

The effects of sawdust addition on the physical and mechanical properties were investigated in this study. Ball clay and kaolin clay were examined in sawdust at weight percentages of 0. 2, 5, 4, 8, and 10 wt.%. The specimens of ceramic bricks were fired at temperatures of 900 °C, 1000 °C, and 1100 °C, and their densities, apparent porosities, water absorption, phase and thermal properties and compressive strengths were evaluated. It was hypothesised that the composition of quartz, mullite, muscovite, and kaolinite in ceramic brick would enhance its properties. The FTIR analysis revealed that Si-O bonding, a silica compound formed within the ceramic brick, is thought to generate a network that imparts rigidity and strength to the ceramic matrix. The TGA revealed the thermal properties of ceramic brick and the weight loss of the specimens. As demonstrated by the experimental outcomes, sawdust decreases the specimen's density and compressive strength. An observation was made regarding the apparent porosity, which showed a 40% increase when sawdust content was increased to 10 wt.% and fired at 900 °C. The ceramic brick containing 2.5% sawdust fired at 1100 °C exhibits a more excellent compressive strength value. Additionally, water absorption increased as the weight percent of sawdust added increased to 10 percent. The findings proved that sawdust waste could potentially be utilised in producing raw clay bricks as a lightweight ceramic brick and pore former.

Keywords: Ceramic brick, Sawdust, Firing temperature, Physical properties, Mechanical properties

TABLE OF CONTENTS

DECLARATION ..... **ii**

ACKNOWLEDGEMENT ..... **iii**

ABSTRAK ..... **iv**

ABSTRACT ..... **v**

TABLE OF CONTENTS ..... **vi**

LIST OF TABLES ..... **x**

LIST OF FIGURES ..... **xi**

LIST OF ABBREVIATION ..... **xiii**

LIST OF SYMBOLS ..... **xiv**

CHAPTER 1

INTRODUCTION **1**

1.1 Background of Study 1

1.2 Problem Statement 3

1.3 Objectives 5

1.4 Scope of Study 6

1.5 Significances of Study 6

CHAPTER 2

LITERATURE REVIEW **8**

2.1 Introduction 8

2.2 Ceramic Brick 8

2.3 Ceramic Brick Raw Materials 9

2.4 Porous Ceramic 9

2.5 Pore Forming Agent 10

2.6 Sawdust 11

2.6.1 Physical Properties and Composition of Sawdust 12

2.7 Firing Temperature 14

2.8 Porosity 14

2.9 Characterization Technique 15

2.9.1 X-ray diffraction (XRD) 16

2.9.2 Fourier Transform Infrared Spectroscopy (FTIR) 17

2.9.3 Thermogravimetric Analysis (TGA) 19

2.9.4 Density, Water Absorption and Porosity 20

2.9.5 Compressive Strength 21

CHAPTER 3

MATERIALS AND METHODS 23

3.1 Introduction 23

3.2 Research Flowchart 24

3.3 Raw Materials 25

3.4 Sample Preparation 26

3.4.1 Mixing 26

3.4.2 Molding 27

3.4.3 Firing 27

3.5 Sample Characterization 28

3.5.1 X-ray Diffraction (XRD) 28

3.5.2 Fourier Transform Infrared Spectroscopy (FTIR) 28

3.5.3 Thermogravimetric Analysis (TGA) 29

3.5.4 Density, Water Absorption and Porosity 29

3.5.5 Compressive Strength Test 31

CHAPTER 4

RESULTS AND DISCUSSION 32

4.1 X-ray Diffraction (XRD) 32

4.2 Fourier Transform Infrared Spectroscopy (FTIR) 37

4.3 Thermogravimetric Analysis (TGA) 40

4.4 Physical Properties of Ceramic Brick 45

4.4.1 Density 45

4.4.2 Porosity 48

4.4.3 Water Absorption 51

4.5 Mechanical Properties of Ceramic Brick 55

4.5.1 Compressive Strength Test 55

4.6 Relationship between composition, physical and mechanical properties 58

CHAPTER 5

CONCLUSION AND RECOMMENDATIONS 60

5.1 Conclusion 60

5.2 Recommendation 61

REFERENCES 62

APPENDIX A 73

APPENDIX B 76

APPENDIX C 81

LIST OF TABLES

Table 2.1: Physical properties of sawdust..... 13

Table 2.2: Compressive strength of sawdust..... 13

Table 3.1: The composition of raw materials with varying of ball clay and sawdust ... 26

LIST OF FIGURES

Figure 2.1: Sawdust.....12

Figure 2.2: XRD analysis: (a) red clay powder (b) sawdust powder.....16

Figure 2.3: FTIR spectra for raw (a) soil and (b) sawdust samples.....18

Figure 2.4: DTA-TGA curve.....20

Figure 2.5: Compressive strength, bulk density, porosity and water absorption of brick made of soil with varying % of sawdust.....21

Figure 2.6: Compressive strength of fired clay bricks.....22

Figure 3.1: Research flow for ceramic brick sample separation and characterization...24

Figure 3.2: Graph of ceramic brick firing process.....27

Figure 4.1: XRD pattern of different various sample fired at 1000°C..... 34

Figure 4.2: XRD pattern of different various of sample fired at 1100°C.....36

Figure 4.3: FTIR spectra of different various of sample fired at a) 1000 °C and b) 1100 °C.....39

Figure 4.4: TGA spectrum of ball clay…….....40

Figure 4.5: TGA spectrum of kaolin clay…….....41

Figure 4.6: TGA spectrum of sawdust…….....42

Figure 4.7: TGA spectrum for various sample.....….....44

Figure 4.8: Density value of various sample fired at 900 °C…….....45

Figure 4.9: Density value of various sample fired at 1000 °C…….....….....46

Figure 4.10: Density value of various sample fired at 1100 ….....47

Figure 4.11: Apparent porosity of various sample fired at 900 °C….....….....48

Figure 4.12: Apparent porosity of various sample fired at 1000°C ….....49

Figure 4.13: Apparent porosity of various sample fired at 1100 °C…….....51

Figure 4.14: Water absorption of various sample fired at 900 °C….....52

Figure 4.15: Water absorption of various sample fired at 1000 °..... 53

Figure 4.16: Water absorption various sample fired at 1100 °C…….....54

Figure 4.17: Compressive strength of various sample fired at 900 °C.....56

Figure 4.18: Compressive strength of various sample fired at 1000 °C…….….....57

Figure 4.19: Compressive strength of various sample fired at 1100°C….....58

Figure 4.20: The relationship between apparent porosity (%) and compressive strength (MPa) fired at 900,1000°C and 1100°C…….....…60

LIST OF ABBREVIATION

XRD	X-ray Diffraction
FTIR	Fourier Transform Infrared Spectroscopy
TGA	Thermogravimetric Analysis
Al	Aluminium
Si	Silicon
O	Oxygen
OH	Hydroxyl group
Fe	Iron
Ca	Calcium
Mg	Magnesium
K	Potassium
Ti	Titanium
Mn	Manganese
CH	Methane (hydrocarbon)
CO	Carbon monoxide

LIST OF SYMBOLS

%	Percentage
wt.%	Weight percentage
°C	Degree Celsius
°F	Degrees Fahrenheit
°	Diffraction angle
θ	Theta
cm^{-1}	Centimeter inverse
g/m^3	Gram per cubic meter
MPa	Megapascal
µm	Micrometer

CHAPTER 1

INTRODUCTION

1.1 Background of Study

Bricks are among the first building materials, extending back to 7000 BC. They are formed of ceramic-based materials, and they remain one of the most often used because they are affordable, manageable, and aesthetically pleasing. At the remains of an ancient building, brick was found in southern Turkey. Clay bricks are employed in load-bearing buildings such as piers, footings, partitions, external and interior walls, and walls (Duggal, 2008). The development of civil engineering may have its roots in the past of masonry construction. Stone, which was easily accessible, was the first building material employed by humans.

Porous ceramic is found in a variety of pore structures, including multilayer materials, foam and honeycomb structures, and micro and mesoporous materials. According to (Wu et al. (2018), these outstanding qualities include low density but high mechanical and physical strength, low thermal conductivity with a high melting point, and good corrosion resistance. Based on the structures, applications are made to the filtration and separation, diffusion, and purification processes. As a result, the technology is also being applied widely in fields like membrane separation, biomedical scaffolding, thermal insulators (Wu et al., 2018), and diesel specific filters (Luyten, Mullens & Thijs, 2010).

Masonry structures seem royal in addition to providing a study base that can survive natural disasters like wind, flood, earthquake, and fire. A few procedures were applied over time to improve the bricks' quality. In the initial stages of sun-baked brick production, chopped straw and grass were incorporated into the clay mixture to inhibit deformation and fracturing. The subsequent notable advancement took place in brick buildings around 4000 BC (Almssad et al.,2022). Fire strengthened brick's tensile strength and longevity.

Clay bricks are still used today for many purposes. To make a brick that has been fired from clay, lightweight and with less heat conductivity, it should have a significant amount of porosity. The primary component in ceramic applications, clay, will offer good plasticity for body shaping. Since the current study is interested in new building materials, the improvement is made using sawdust waste. Clay brick production requires firing temperature. It affects clay brick physical, texture, and mineralogical formation (Phonphuak..,2020).

Sawdust is a by-product of basic woodworking. To create a lightweight ceramic brick from clay, the pore-forming agent employed is sawdust. Cellulose, hemicellulose, and lignin are the three primary substances of wood that makeup sawdust. These combined components give the microstructure of the clay more porous. The bulk of the chemical elements in sawdust where 60.8 %, 5.2 %, 33.8 %, and 0.9 %, respectively are carbon, hydrogen, oxygen, and nitrogen (Horisawa et al., 1999). In ceramics technology, the sawdust waste can be mixed into clay because sawdust is the preforming agent. The fired clay microstructure is more porous due to the combination of these elements. As a result, the clay loses density and improves its capacity for thermal insulation. Around 1050 °C has been discovered to be the ideal sintering temperature (Johari et al. 2010).

Okunade, (2008) investigated the use of sawdust and ash wood in laterite-clay bricks. The materials utilised in the study were sawdust from burning fire and wood ash in a 70:30 weight-to-laterite clay ratio. The mixes are then added in various ratios, ranging from 0 to 10%. According to the study, this led to good in denser with high compressive strength that contained (0% sawdust and 10% wood ash). The research stated that wood ash was made up of lighter and more porous substances.

By studying different composition of sawdust, the mechanical and physical properties of ceramic bricks were investigated. Once the sawdust composition was optimised it was fired for three different temperatures to determine the combustion behaviour, physical characteristics, and mechanical characteristics that result in the highest performing fired clay bricks. X-ray Diffraction (XRD), Fourier Transform Infrared Spectroscopy (FTIR), Thermogravimetric Analysis (TGA), density, apparent porosity, water absorption, and compressive strength of the ceramic brick will characterize.

1.2 Problem Statement

Clays are burnt at high temperatures to form a dense, hard material that is used to make ceramic bricks, a particular kind of building material. They are frequently utilised in building due to their tenacity, procedure, to tolerate high temperatures, and qualities of thermal and acoustic insulation. The issue here is rising demand for clay bricks with better insulation. So, one of the solutions to solve this problem is to promote the porosity in the clay body. The most common organic pore formers include sawdust, polystyrene, paper muck, coal, and coke. In previous study, there is a significant quantity of sawdust is being added to the ceramic bricks composition which consist of raw-brick clay. The sawdust act as the pore-former that was produced porosity in the

ceramic bricks. Porosity is one of the factors that reduce the density (Phonphuak et al., 2016). However, the higher amount of the sawdust was reduced the compressive strength of the ceramic bricks. The porosity in the ceramic bricks act as barriers to heat transfer by reducing the density of the material and creating a pathway for air to flow and this was reduced the thermal conductivity. The large amount of sawdust was caused crack in the sample body. The usage of ball clay and kaolin clay due to the particle size enhanced the physical and mechanical properties than use of single clay and also effect the interlocking of ceramic bodies. (Bwayo & Obwoya., 2014).

Sawdust has inconsistent particle size and morphology where it is difficult to control the porosity and mechanical properties of the insulator at the same time (Ali et al., 2017). The by-product's particle size influences the porous ceramic's mechanical and physical strength. Following the complete burning of the byproduct, pores will form. Therefore, the pore and its size distribution will influence the mechanical and physical characteristics of porous ceramic. As a result, by adjusting the initial size of sieved sawdust used as a pore-forming agent, the pore and size distribution of porosity can be controlled. Therefore, the inconsistent sizeof particle distribution and pore forming can be overcome (Bwayo & Obwoya., 2014).

Sawdust is the best material to be utilises because it can be used to make lightweight ceramic bricks. Wood sawdust has a fine and uniform particle size distribution ranging from 1.5 µm to 63 µm, so it may be used as a pore-forming agent for thermal insulators (Barcenas et al., 2005; Aramide, 2012). Furthermore, wood sawdust has a significantly lower ignition point, ranging from 118 to 142 °C (Kotoyori 1986). In earlier studies (Phonphuak., (2020) stated that the fire temperature caused using sawdust waste caused the specimens bulk density and compressive strength to decrease. In the production of ceramic bricks, the ceramic bricks must have a high

compressive strength to use at the construction area but in this case the ceramic brick that without addition of sawdust are high in strength than with the addition of different quantities of sawdust. Since sawdust waste has a lower density and a higher porosity than clay, (Phonphuak., (2020) recognises that clay bricks compressive strength decreases as sawdust waste content increases. However, theoretically, firing at a higher temperature could result in ceramic having a good mechanical and physical properties.

To identify the composition of sawdust as additives and the effect firing temperature to mechanical and physical properties of ceramic bricks, this study was conduct with 900 °C, 1000 °C and 1100 °C firing temperatures and 0, 2.5, 4.0, 8.0 and 10 wt.% composition of sawdust added to raw brick clay body. In this study, kaolin was added to prepare the raw brick clay body to study difference that may occur during the process, because kaolin has good plasticity, meaning it can be easily molded and shaped into the desired form. This research take place to ensure that the ceramic bricks produced from materials are economical and environmentally friendly (Ahmed et al., 2018). The byproduct offers an eco-friendly and efficient method of disposal, as well as enhanced physical and mechanical properties.

1.3 Objectives

The objectives of this study are:

i. To prepare the ceramic bricks by using different kind of clays (ball clay and kaolin clay)
ii. To identify the effects of adding sawdust as additives.
iii. To study the effect of firing temperature to mechanical and physical properties of the ceramic bricks.

1.4 Scope of Study

The addition of raw material composition was result in the production of the ceramic brick. Ball clay has a weight percentage of 100, 72.5 ,71.0 ,67.0, and 65.0 while kaolin clay has a consistent weight percentage of 25 respectively. Sawdust was 0, 2.5, 4.0, 8.0 and 10 wt.%. Five distinct samples were created for this study using five different sawdust compositions. After the firing process, the impact of adding various amounts of sawdust composition was examined. Moreover, the other parameter in this study is the firing temperature. The five difference compositions were undergo three firing temperature which are at 900 °C, 1000 °C and 1100 °C with soaking time for 1 hour to identify the mechanical and physical properties of the ceramic brick. All the samples were characterized by XRD, FTIR, TGA density, porosity water absorption, and compressive strength to analyse the physical and mechanical properties of ceramic bricks. The techniques, phases and properties can be analysed by using all this characterization.

1.5 Significances of Study

Extreme weather resistance is a property of ceramic bricks. However, they may be impacted in the following ways by weather changes. Ceramic bricks can absorb some water when exposed to moisture or water. Bricks may crack or spall if the temperature falls below freezing because the water inside them may freeze and expand. Ceramic bricks may expand because of heat in hot, dry conditions. The bricks may shatter or crack if the temperature changes rapidly (Santa et al.,2023).

According to (Santa et al., (2023) ceramic bricks can collect moisture from the air in areas with high humidity levels. This may result in efflorescence, a white powdery

substance that develops on the surface of bricks. Moreover, the sawdust as additives reduces the compressive strength of ceramic bricks because of the high porosity but the strength can increase by firing to high temperature. It is crucial to guarantee the ceramic bricks strength so they can endure external loads and keep their structural integrity. If a bricks compressive strength is insufficient, it could break or even collapse beneath the weight of the building. Ceramic bricks are used in building to give a structure long-lasting resilience. As a stronger brick is more resistant to damage and wear and tear, the compressive strength of a brick directly correlates to its durability. Sawdust may enhance ceramic brick porosity and high firing temperatures may strengthen ceramic bricks (Johari et al.,2010).

The finding of this research gives the lightweight ceramic bricks because of the porosity that produce from the sawdust. Besides, this study was used to encourage the usage of eco-friendly materials and recyclable. At the same time, this study can provide the optimum weight percentage of sawdust respective with good mechanical and physical properties of the ceramic bricks.

CHAPTER 2

LITERATURE REVIEW

2.1 Introduction

This chapter introduces the function and properties of the ceramic brick. Furthermore, the selection of materials for manufacturing ceramic bricks was based on their specific types of clays, additives, function, properties, and advantages. The suitable firing temperature required to achieve the desired properties of ceramic bricks is also being discussed. The ceramic brick samples were analysed using relevant characterization techniques following the firing process.

2.2 Ceramic Brick

A common building material of ceramic brick is ceramic, which is composed of a mixture of minerals, primarily clays, and up to 30 wt.% water. Bricks are fired at a higher temperature and produce a glassy product with enhanced density, strength, and hardness as well as increased resistance to chemicals and cold. Although this temperature can be reduced by drying process before firing from 30 % to 25 %, water is pushed off during fire. As (Kornelia Wiśniewska et al., (2021) stated that reduced water content is formed as powder and fired for days or weeks at 1,800 - 2,000 °C, based on the ceramic's composition and the specifics of the firing procedure. Ceramics may be painted or may have a fired appearance. These materials won't further oxidise in the air

and are ecologically stable, the maintenance is inexpensive. They are more prone to problems when combined with other materials, typically fasteners that are stressed and corrode-prone. If repairs fail, a serious situation can develop. In contrast to metals, ceramics do not exhibit ductile behaviour. They crumble brittlely after exceeding their elastic limit. (Bwayo & Obwoya., (2014) combined ball clay and kaolin clay used to make ceramic bricks, and each of the raw materials' unique compositions plays a crucial part in ensuring the excellent quality of the finished product.

2.3 Ceramic Brick Raw Materials

Kaolin clay and ball clay are the basic materials used for producing ceramic bricks. Each basic material contributes to the quality of the final product in a unique manner. First, kaolin clay ($Al_2Si_2O_5(OH)_4$) impart plasticity and function as a body former. Next, ball clay ($Al_2O_32SiO_22H_2O$) is one of the earth materials with very fine particle size that functions as the primary binder in the ceramic composition. In addition, the addition of sawdust to the ceramic bricks during the firing process ensures their mechanical and physical properties. The various compositions of each brick's raw materials influence the final product.

2.4 Porous Ceramic

A few investigations carried out recently have shown that it is possible to use industrial waste to make ceramic products, particularly porous ceramic products. (Gorhan & Şimşek.,2013). In general, ceramics are produced from natural raw materials with very heterogeneous chemical and mineralogical compositions, which are similar to the compositions of many types of waste. This similarity makes them very suitable to be

used as alternative raw materials (Barbieri et al.,2013). Porous ceramics, as a class of highly reticulated ceramic materials, are generally found in a variety of pore structures, including foam and honeycomb structures, multilayer materials, and micro- and meso-porous materials (Zakaria et al.,2020). This similarity makes them very suitable to be used as alternative raw materials in the production of various ceramic materials, especially porous ceramic materials. In the last decade, porous ceramics have stood out due to their wide possibilities for use in various fields of engineering, ranging from filtration and water treatment to thermal or acoustic insulation and catalytic support. (Yatim & Rahman.,2020). Nowadays, a class of extremely reticulated ceramic material known as porous ceramics includes a variety of structures, including foams, honeycombs, interconnected rods, fibres, and hollow spheres. Because of their special blend of advantageous characteristics, including porosity, water absorption, and modulus of rupture (MOR), porous ceramics are useful in both traditional and cutting-edge engineering applications.

Porous ceramics can generally be used as filtration materials to remove harmful bacteria from microorganisms. The products produced from increasing the degree of fine-pore control in porous ceramics become more significant and valuable over time, increasing the use of porous ceramics in separation, dispersion, and adsorption technologies (Bose & Das.,2014).

2.5 Pore Forming Agent

Mineral and renewable resources are the two categories into which pore-forming agents can be divided because of their non-toxicity and economic value, natural pore-forming agents like wheat straw, rice husk ash, and many others are widely used to fabricate porous ceramic (Zakaria et al.,2020). Still, it is rather difficult to control the

ceramic's porosity and mechanical qualities at the same time because the natural agent's irregular particle size and morphology (Borredon et at., 2014). Numerous pore-forming agents exist, including rice hush ash, wheat straw, and others (Beal et al., 2019). As a result, heat will be trapped and insulated inside of it via pore formation. A thermal insulator has a low thermal conductivity and is a poor heat conductor. According to Pacheco-Torgal et al. (2015), insulation is used in manufacturing processes and buildings to stop heat gain or loss.

According to studies, the insulator's pores function as voids or empty spaces to insulate heat flow, even though they might also contain air (Ranjani et al., 2009). As a result, the insulator's thermal conductivity is reduced. Developing porous ceramic insulators is imperative because they need superior mechanical properties, a minimum amount of water absorption, an ideal pore-size distribution, and proper property balancing. Given this stringent requirement, (Sutcu and Akkurt., (2009) found that synthetic materials like carbon, oil shale (OS), expandable polystyrene (EPS), tert-butyl alcohol (TBA), polymer microbeads, and carbon make up the majority of the pore-forming agents in insulators.

2.6 Sawdust

Wood sawdust is one of the most common byproducts of wood exploitation and processing, including sawing, milling, planning, routing, drilling, and sanding as shown in Figure 2.1. Sawdust is a pore forming agent where form pores and produce a lightweight ceramic brick. Addition of sawdust alter the mechanical and physical properties because sawdust act as the filler. The burgeoning lumber industry, furniture companies, and other sources produce significant amounts of sawdust and sawmills in Malaysia and other emerging nations. It could be a significant contributor to

environmental pollution if stored under uncontrolled conditions (Deac et al.2016). Traditionally, wood dust is used as furniture, medium density fibreboard (MDF), solid fuel for boilers, and some is eventually disposed of in landfills (Thetkathuek et al., 2010). However, the volume of sawdust produced each year is so great that those applications and efforts are still insufficient (Ratnasingam et al., 2010). Therefore, the objective of this investigation is to identify the mechanical and physical properties in addition of sawdust in ceramic brick.

Figure 2.1: Sawdust

(Source: Sohail et al., 2017)

2.6.1 Physical Properties and Composition of Sawdust

Sawdust is created when wood is processed for a variety of purposes. Depending on the type of tree that is being treated, its makeup differs greatly. Sawdust mostly contains cellulose (between 40 - 50 wt. %), polyoses, lignin, and a vast and diverse range of molecules with a lower relative molecular mass, which may have a major impact on the qualities of the wood (Humans, 2012). The particle size, or surface morphology, smell, and density of wood sawdust are its primary physical characteristics. Different breeds of wood come in a variety of colours, ranging from white - aspen, spruce) to black - ebony. The colour, lustre, smell, and particle size of the

wood sawdust can all be evaluated visually. Table 2.1 and Table 2.2 shows the physical properties of sawdust and compressive strength of sawdust.

Table 2.1: Physical properties of sawdust.

(Source: Demir, 2008)

Physical Properties	**Sample series of sawdust**			
	A (0%)	B (2.5%)	C (5%)	D (10%)
Bulk density (g/cm3)	1.80	1.56	1.45	1.35
Apparent porosity (% vol.)	30	33.4	37.5	42.2
Apparent density (g/cm3)	2.42	2.21	2.14	1.98
Water absorption (% wt.)	16.65	21.40	25.80	31.25

Table 2.2: Compressive strength of sawdust.

(Source: Demir, 2008)

Compressive strength (MPa)	**Sample series of sawdust**			
	A (0%)	B (2.5%)	C (5%)	D (10%)
Fired samples	15.5	13.60	11.35	9.85
Unfired samples	2.6	3.35	4.40	5.10

2.7 Firing Temperature

Ceramic brick typically has a high melting point and ceramic bricks are made from raw materials like clay which are then heated to extremely high temperatures. The materials chemically bond with one another during the firing process to create strong and durable material. However, the most ceramics typically have melting temperatures between 1200 °C and 1600 °C (2192 °F and 2912 °F). According to (Eliche-Quesada et al., (2012), the higher firing temperatures result in higher-quality bricks because the firing procedure increases the bricks' resistance to compression. The firing temperature effects the ceramic brick's porosity, strength, and durability. If the temperature is too low, the bricks may not be fully densified and have higher porosity, making them more prone to breakage and damage. On the other hand, if the temperature is too high, the bricks may become overly dense and brittle, which can also affect their strength and durability. According to Phonphuak., (2020), the ceramic brick sample were fired at a temperature of 900 °C, 1000 °C and 1100 °C with 30 minutes soaking time were able to obtain the effects of temperature on mechanical and physical properties of ceramic bricks can be studied over time. The samples are kept at the highest firing temperature around 1100 °C during the soaking time to allow chemical reactions that take place during the firing process to finish.

2.8 Porosity

Ceramic brick usually contains considerable porosity in their body. The number of pores or empty space that a substance contains is referred to as its porosity. A ceramic bricks porosity might change based on the materials used and the

manufacturing process. A ceramic brick porosity may have an impact on its strength, tenacity, and thermal insulation.

To improve the material's capacity to collect and release gases or moisture as well as its thermal insulating qualities, a certain amount of porosity might also be advantageous. Ceramic bricks can be produced using a variety of methods, such as adding pore-forming like sawdust or regulating the fire temperature and duration, to meet certain porosity requirements. Moreover, these bricks have a higher porosity than conventional ceramic bricks, which results in a lighter weight with comparable thermal insulating capabilities (Farnood Ahmadi et al. 2018).

Phonphuak., (2020) stated that the results were variable in apparent porosity depending on the inclusion of sawdust. For a 10 wt. % sawdust addition and firing at 900 °C, the highest porosity was around 32.40 %. Bricks with a 2.5 wt. % sawdust content that were burned at 1100 °C had the lowest porosity, 22.80 %. So, when the sawdust addition was burned out during the firing process, the porosity in ceramic brick was produced. Therefore, a higher sawdust content in ceramic brick result in a higher open porosity, which then generate more porous ceramic brick and lighter ceramic.

2.9 Characterization Technique

The ceramic brick, which has been fired and contains sawdust, undergo various characterization techniques to determine its structure, chemical composition, elemental composition, compound composition, bonding, and physical and mechanical properties.

2.9.1 X-ray Diffraction (XRD)

X-ray Diffraction (XRD) is a technique that can be employed to determine the distinct phases and crystalline structures that exist within a material. X-ray diffraction (XRD) can identify the mineral composition of a fired sample. According to the study (Jannat et al., (2021)., the XRD pattern of clay revealed quartz to be the dominant mineralogical phase. Haematite (Fe_2O_3) and kaolinite ($Al_2Si_2O_5(OH)_4$) were two other mineral phases found in the clay. However, the disordered XRD pattern showed hemicelluloses and lignin in the sawdust. Cellulose was the only crystalline phase found, and it showed a wideband peak at 35 °, 22.6 ° and 15–18 ° as shown in Figure 2.2 (Jannat et al. 2021).

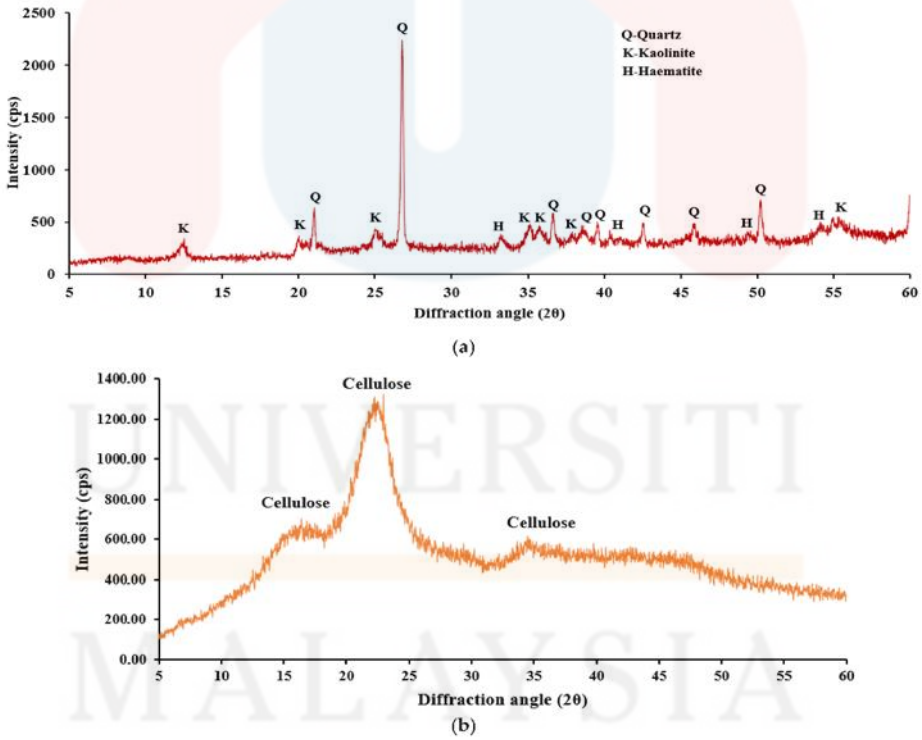

Figure 2.2: XRD analysis: (a) red clay powder (b) sawdust powder.

(Source: Jannat et al. 2021)

2.9.2 Fourier Transform Infrared Spectroscopy (FTIR)

FTIR analysis is employed to examine electromagnetic radiation within the infrared portion of the spectrum. FTIR can be used to determine ceramic materials molecular structure and chemical composition based on bonding type and functional groups. Several functional groups in clay minerals, such as hydroxyl, carbonate, and silicate, can be found and measured using FTIR. These functional groups can provide information about the substances chemical bonding and intermolecular interactions. The researcher (Shafiquzzaman et al.,(2022) discovered bands of quartz-rich soil at 1084 cm^{-1}, 741cm^{-1}, 699 cm^{-1}, and 471 cm^{-1}. At 800–400 cm^{-1}, potassium, sodium, and calcium aluminosilicates combine to create feldspar. The absorption bands at 983 cm^{-1} in the soil samples indicated sulphates. Soil samples were analysed utilising 741 cm^{-1} vibration bands to find dolomite. The FTIR spectra of carbonates were 1790-1820, 1400-1500, 870, and 741 cm^{-1}. The vibrational range of hematite (a ferrous oxide) is 440–400 cm^{-1}. Kaolinite absorption bands were 3688, 3624, 3615, 905, 699, and 471 cm^{-1}. 471 cm^{-1} absorption spectra show Si-O. Because of the magnesium-rich chlorite or OH-adsorbed water, both samples displayed distinct 1640–1600 cm^{-1} spectra. Because of hydroxyl linkage (O-H), the soil sample shows different bands between 3400 and 3750 cm^{-1}.

Clusters of cellulose, lignin, and phenol were discovered in sawdust at 3291 cm^{-1}. Uneven vibrations of CH_2 and CH_3 resulted in a vibration band of 2850 cm^{-1}. Samples of sawdust had a carboxylate cluster at 1587 cm^{-1}. Pectin (-COOH) is visible in the vibration band at 1328 cm^{-1}. The vibration of hemicellulose is 1213 cm^{-1}. As shown in Figure 2.3, the sawdust sample has the halogen group C-X (Shafiquzzaman et al., 2022).

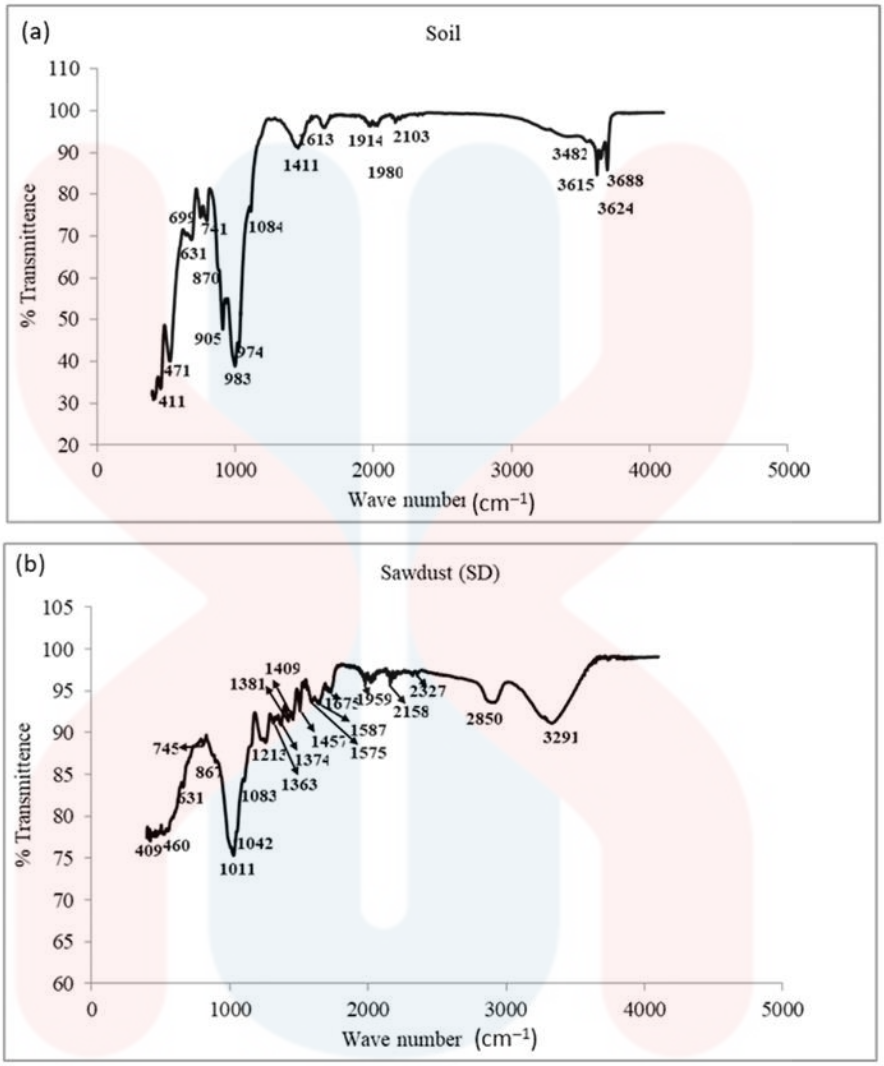

Figure 2.3: FTIR spectra for raw (a) soil and (b) sawdust samples.

(Source: Shafiquzzaman et al. 2022)

2.9.3 Thermogravimetric Analysis (TGA)

Thermogravimetric Analysis (TGA) is a technique used to investigate materials thermal stability. The sample undergoes multiple thermal transitions as the temperature increases, such as dehydration, decomposition, and oxidation, which changes in the sample's mass can be detected. The results of the TGA analysis may provide information about the thermal behaviour of the sample. The thermal stability of the clay employed in producing ceramic bricks can be assessed using Thermogravimetric Analysis (TGA). The clays thermal stability is a crucial determinant of the highest temperature at which bricks can be fired without experiencing any structural harm (Vasconcelos da Silva et al.,2020)

Additionally, TGA can be used to analyse contaminants or additional additives found in glaze or clay materials. The initial observation in the TGA curve results from the previous researcher's investigation of water evaporation when yellow clay and grey clay with sawdust are combined. The water evaporation process begins at temperatures surpassing 50 °C and persists until approximately 200 °C. The primary outcome is the combustion of sawdust particles within the temperature range of 270 - 620 °C. The process by which kaolinite is converted to metakaolinite through the liberation of OH- has lower across this range of functional groups. An additional increase in temperature initiates the decomposition process of the carbonates. Carbonates function as agents that form pores and generate crystalline phases when exposed to fire, thereby potentially enhancing mechanical strength. According to the CO_2 partial pressure, calcium carbonate decomposes at approximately 700 °C and reaches 860 °C. Figure 2.4 shows the DTA-TGA analysis did not establish conclusive evidence of liquid formation. Water evaporation is the primary cause of weight loss in the production of bricks. (Thalmaier et al., 2020).

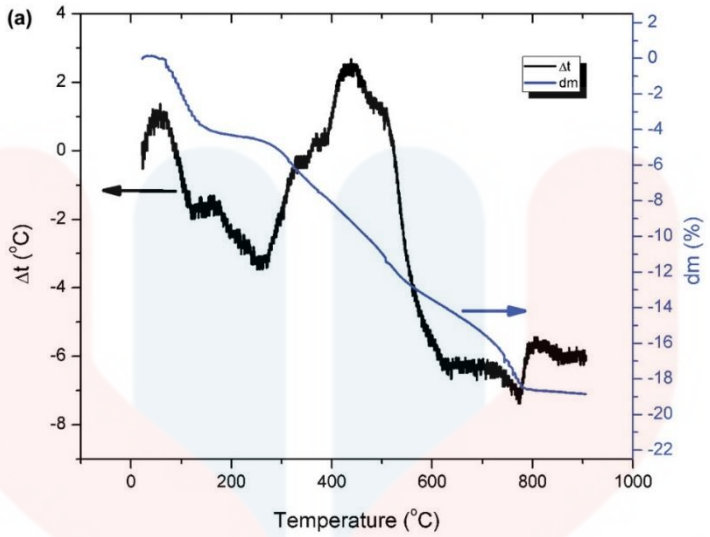

Figure 2.4: DTA-TGA curve

(Source: Thalmaier et al., 2020)

2.9.4 Density, Water Absorption and Porosity

The apparent porosity of the porous ceramic brick was increased by incorporating a byproduct that is produced during the firing process (Cotes-Palomino et al., 2015). The ceramic brick's water absorption and apparent porosity were directly proportional to its porosity. Conversely, the bulk density decreased, leading to increased porosity and a decrease in bulk density due to the process.

Accordingly, the ability of ceramic bricks to absorb water increases when byproducts are added (Demir, 2008). Earlier studies (Demir., (2008) have shown that the inclusion of sawdust decreased bulk density, reducing it from 2.01 to 1.25 g/m^3. Including sawdust they resulted in a 7.4 % increase in the apparent porosity, bringing it to 56.7 %. Additionally, the water adsorption capacity increased by 3.75 to 45.4 %. According to Shafiquzzaman et al. (2022), the presence of sawdust reduced compressive strength and bulk density, as illustrated in Figure 2.5.

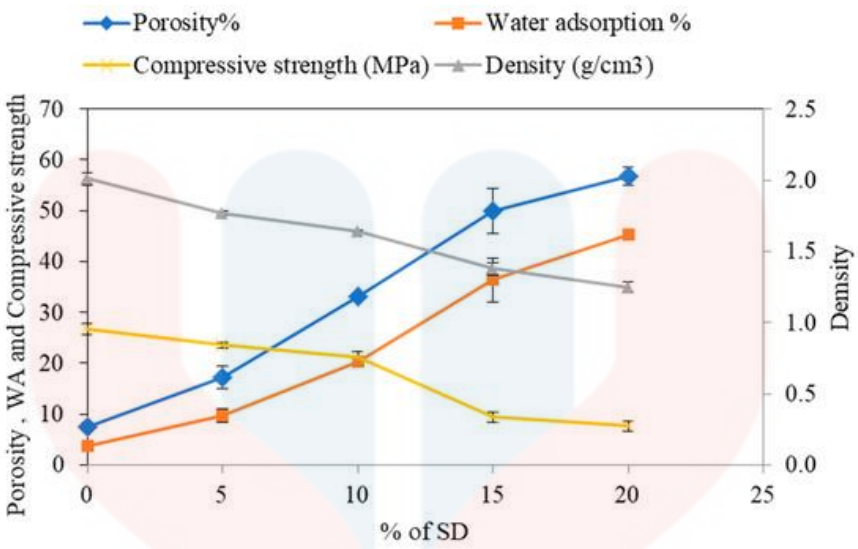

Figure 2.5: Compressive strength, bulk density, porosity, and water adsorption of bricks made of soil with varying % of sawdust.

Source: (Shafiquzzaman et al. 2022)

2.9.5 Compressive Strength

The sample undergoes complete crushing during the compressive test, and the young modulus of rupture is recorded. The machine measures the young modulus, maximum force, stress, and strain of the sample after its placement on the holder. Phonphuak's (2020) demonstrated that an increase in sawdust waste led to a decrease in the compressive strength of clay bricks. This was attributed to alterations in porosity and density. By increasing the temperature at which firing occurs, the porosity level is decreased while the thickness is augmented, leading to a notable improvement in compressive strength. The compressive strength of fired clay bricks is higher at 1100 °C than at 1000 °C. By utilising sawdust waste at a concentration of 2.5–10 percent by weight, the compressive strength was increased from 4.35 to 18.2 MPa. As illustrated in

Figure 2.6, the specimen that produced the most favourable outcomes was fired at 1100 °C with a mixed ratio of 2.5% by weight.

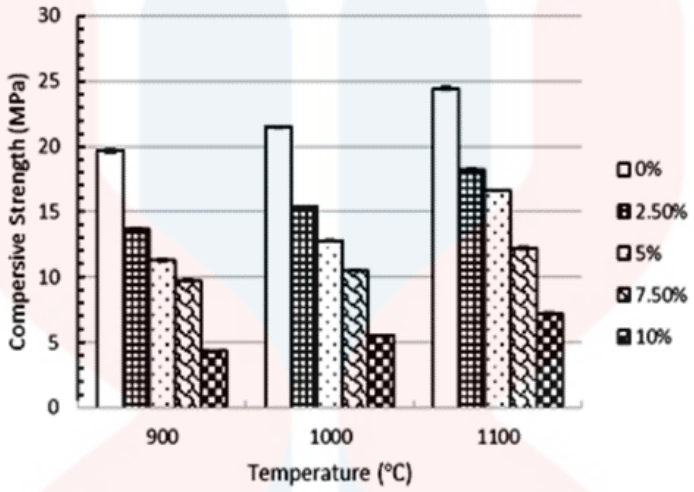

Figure 2.6: Compressive strength of fired clay bricks.

(Source: Phonphuak.,2020)

CHAPTER 3

MATERIALS AND METHODS

3.1 Introduction

This chapter contains an overview of the preparation and characterization of the materials. The ceramic brick is composed of a range of clay variations. A sample of ceramic bricks was fabricated in this investigation utilizing a range of raw material compositions. They were fired at three distinct temperatures to accomplish the intended goals of determining the mechanical and physical properties of the samples. The lightweight ceramic bricks are manufactured through the incorporation of various sawdust additives. Moreover, by employing various characterization techniques, this study identifies changes in physical and mechanical properties.

3.2 Research Flowchart

The research flow chart shows the sample preparation, evaluation and characterization steps as shown in Figure 3.1.

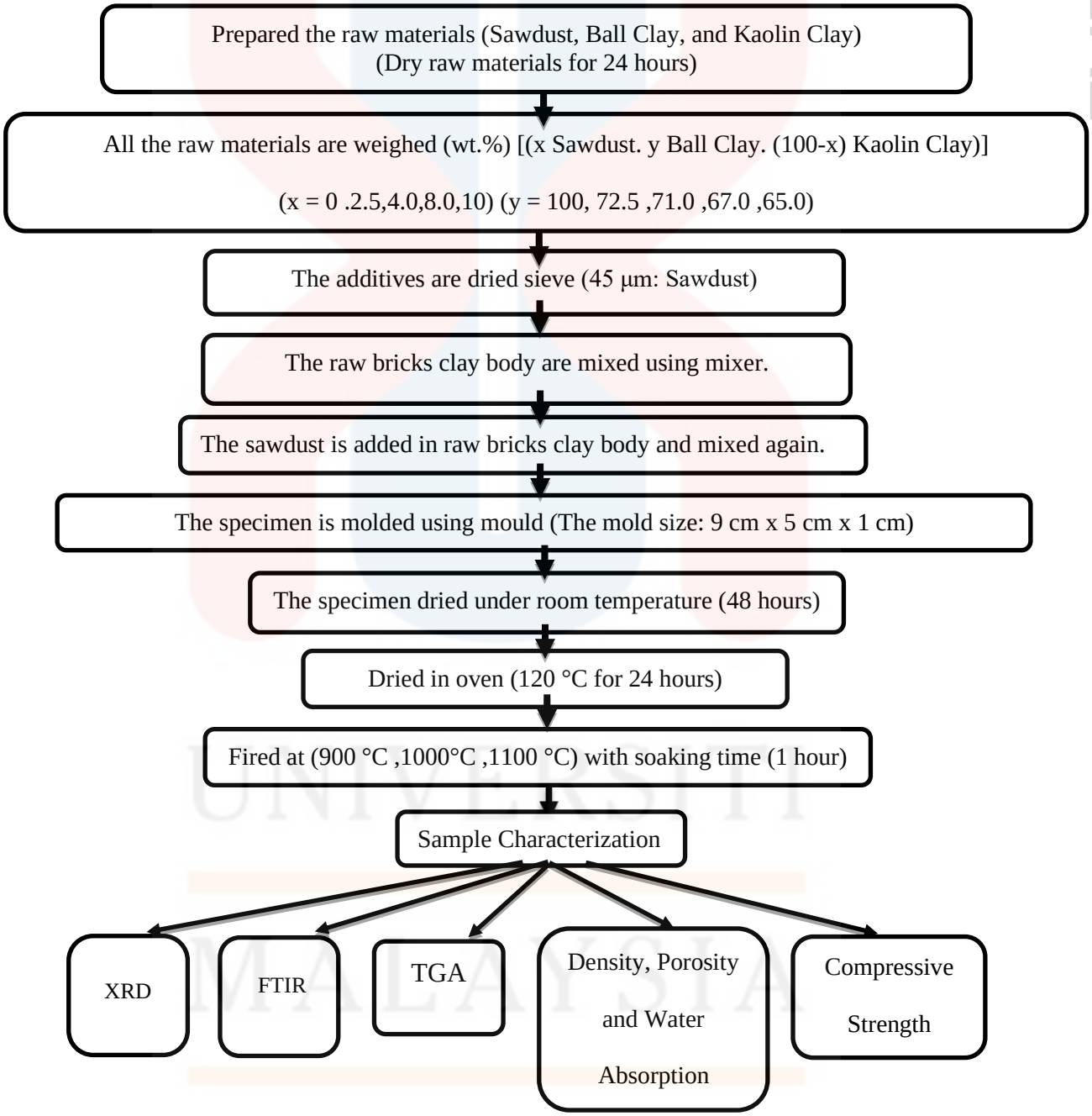

Figure 3.1: Research flow for ceramic brick sample preparation and characterization.

3.3 Raw Materials

Various raw material compositions are utilised to prepare the brick sample. To determine samples physical and mechanical properties, sawdust is added and heated to three distinct temperatures. Different characterization techniques were employed to determine the mechanical and physical properties. China clay makes up 10 percent by weight of the ceramic brick composition, in addition to kaolin clay 15 percent by weight, various weights of ball clay, and sawdust utilized as an additive. Having a soft texture, China clay ($Al_2Si_2O_5(OH)_4$) is a fine-powder substance characterized by its low thermal conductivity and high thermal stability. Ceramic bricks manufactured using kaolin clay [$(Al_2O_3(SiO_2)_2(H_2O)_2)$], which functions as a forming agent and source of plasticity. Ball clay ($Al_2O_32SiO_22H_2O$) is the principal binder material. Sawdust, the concluding component in the ceramic composition, has the potential to augment the material's porosity and render it more lightweight. To attain a uniform particle size of 45 mm, the sawdust is sieved through a mesh measuring 45 μm. The formation of the five unique compositions of ceramic bricks is achieved through the modification of the sawdust composition, as shown in Table 3.1.

Table 3.1: The composition of raw materials with varying of ball clay and sawdust.

Raw Materials	*Sawdust (wt. %)*	*Ball Clay (wt. %)*	*Kaolin Clay (wt. %)*
Control	*0.0*	*100.0*	*0.0*
Sample 1	*2.5*	*72.5*	*25.0*
Sample 2	*4.0*	*71.0*	*25.0*
Sample 3	*8.0*	*67.0*	*25.0*
Sample 4	*10.0*	*65.0*	*25.0*

3.4 Sample Preparation

3.4.1 Mixing

All the raw materials where kaolin clay, ball clay and sawdust are weighted with their different composition as listed in Table 3.1. Then, the raw brick clay body materials are mixed using mixer until it's homogenous for 1 hour. Then sawdust added as pore-former to the raw brick clay body and mixed again using hand for 1 hour too. The sawdust is sieved first to make sure get the fine particles.

3.4.2 Molding

After mixed, the specimen is molded where the mold size is 9 cm x 5 cm x 1 cm, and the specimen was dried under the room temperature for 48 hours. Then, the specimens dried at oven for 24 hours with 120 ℃ temperature.

3.4.3 Firing

The five samples with different composition are fired at a three different temperature which is 900 ℃, 1000 ℃ and 1100 ℃ and using fire rates of 5 ℃ per minutes with soaking time for 1 hour as shown in Figure 3.2. The firing temperature can produce different mechanical and physical properties of samples.

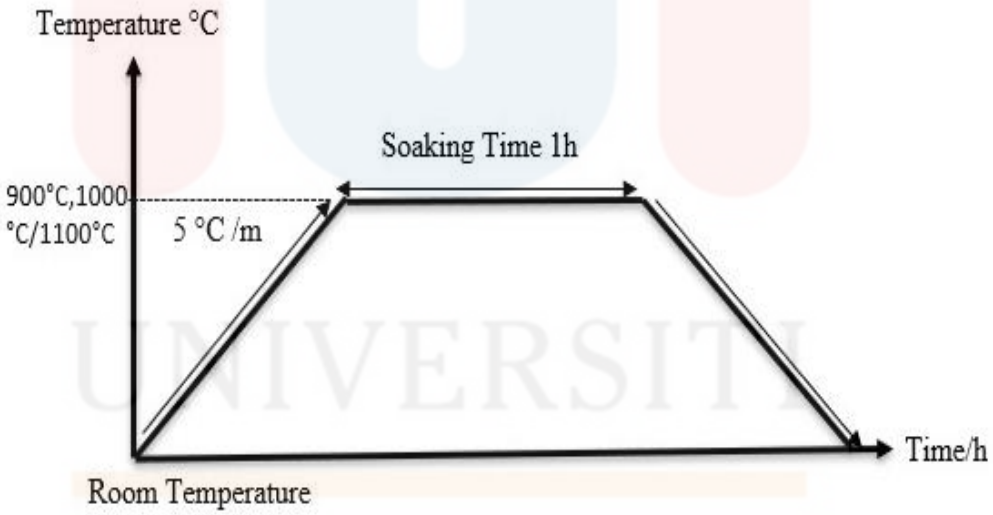

Figure 3.2: Ceramic brick firing profile

3.5 Sample Characterization

3.5.1 X-ray Diffraction (XRD)

The material's distinct phases and crystalline structures can be identified using Bruker D2 Phaser X-ray Diffraction (XRD). In addition, XRD can be used to ascertain the mineral composition of a fired sample. Following the firing procedure, samples are analysed by XRD. In powder XRD application, it is customary to reduce the ceramic brick sample to a fine powder of approximately 2 μm. The powder is subsequently prepared in a sample stage or holder for analysis. Powder XRD is commonly employed to analyse the crystallographic structure and phase identification of ceramic materials. The data were gathered in continuous scan mode for 2θ = 10 ° to 90 ° at a rate of 2 °/min. In XRD patterns, peak intensities indicated the concentration or quantity of a specific crystalline phase within the ceramic brick.

3.5.2 Fourier Transform Infrared Spectroscopy (FTIR)

FTIR using Nicolet iz10 machine, is a technique utilized to quantify electromagnetic radiation in the infrared region. The findings provided insights into the sample's intermolecular interactions and chemical bonds. The FTIR used wavenumbers or wavelengths ranging from 400 to 4000 cm^{-1}, encompassing the electromagnetic spectrum's mid-infrared (MIR) segment. To determine the transition temperature of the ceramic brick, fine powder must be ground into it. During the transition measurement, the sample surface was travelled across by infrared radiation.

3.5.3 Thermogravimetric Analysis (TGA)

Thermogravimetric Analysis (TGA) using HT Mettler Toledo is a technique utilized to investigate the thermal stability Previously, clay and other components utilized in ceramic brick were analyzed using TGA. A temperature was applied to the substance as it was weighed for TGA analysis. As the temperature increased, the sample experienced thermal transitions, such as dehydration, breakdown, and oxidation, as indicated by changes in the sample's mass. The TGA sample must be in powder form with a 5 to 20 milligram mass.

The samples are weighed before characterization and placed in the TGA instrument's crucible. Ceramic bricks are heated at a rate of 10 °C/min. To analyze ceramic brick samples, the temperature was generally increased from ambient to one thousand degrees Celsius or higher, contingent upon the anticipated decomposition characteristics.

3.5.4 Density, Water Absorption and Porosity

The density and porosity were adhered to MS ISO 10545-3: 1995. Water absorption, apparent porosity, and bulk density are ascertained through this characterization. Vacuum measurements were made of water absorption. The water absorption was established utilizing the vacuum method. This technique involves removing air from a chamber containing the samples, followed by submerging the samples in water. The samples were weighed before and after water immersion to compute apparent porosity, water absorption, and bulk density, utilizing the water absorption by using Equation 3.1,3.2 and 3.3.

Water Absorption (%) =

$$\boldsymbol{E(b,v) = (\frac{m2\ (b,v)}{m1} - \frac{m1}{m1}) \times 100}$$ Equation 3.1

Where:

m1: the mass of the dry brick

m2: the mass of wet brick

Apparent Porosity (%) =

$$\mathbf{p} = \frac{m2v}{V} - \frac{m1}{V} \times 100$$ Equation 3.2

Where:

m1: mass of dry brick

m2: mass of wet brick

v: volume

Bulk Density Equation =

$$\mathbf{B} = \frac{m1}{v}$$ Equation 3.3

Where:

m1: mass of dry brick

v: volume

3.5.5 Compressive Strength Test

The compressive strength of ceramic bricks is frequently tested using a Universal Testing Machine (UTM) in accordance with international standards like ASTM C67. The specimens underwent complete crushing throughout the compressive test, facilitating the determination of the juvenile rupture modulus. This test determines the force peak, energy to break, and stress break of the sample. Compressive strength values vary between 4.35 and 18.2 MPa.

CHAPTER 4

RESULTS AND DISCUSSION

4.1 X-ray Diffraction (XRD)

The X-ray diffraction (XRD) patterns of B100S0, B72.5S2.5, B71S4, B67S8, and B65S10 at a temperature of 1000 °C are illustrated in Figure 4.1. According to the literature, quartz, kaolinite, and hematite are the phases that present in ceramic brick made from ball clay, kaolin clay, and sawdust (Jannat et al. 2021). In contrast, the XRD analysis reveals the presence of kaolinite, muscovite, and quartz, as shown in Figure 4. The pattern distribution of the crystallinity of the samples increases from 46.6% for sample B100S0 to 47.9% for sample B72.5S2.5 and decreases marginally from 46.4% for sample B71S4 to 40.9% for sample $B_{67}S_8$. The sample B65S10 exhibits a marginal increase in crystallinity, reaching 41.5%.

Following firing at 1000 °C, the intensity of the kaolinite ($Al_2H_4O_9Si_2$) peak distribution increased from sample B100S0 to sample B65S10. With a peak at 2θ = 19.8°, kaolinite (COD 9009230) exhibits high crystallinity. At high fire temperatures, kaolinite imparts workability and functions as a precursor to the mullite phase in solid-state sintering. The dihydroxylation of kaolinite found in clay minerals would result in its transformation into metakaolinite. The potential consequence of this alteration is a reduction in the prominence of kaolinite peaks and the emergence of more extensive amorphous scattering (Maruoka et al., 2023).

Samples B100S0 through B72.5S2.5 exhibited an increase in the intensity of the quartz (SiO_2) phase. Following a slight decrease at B71S4, the intensity returned at B67S8 and B65S10. Quartz (COD 1011172) exhibits a high degree of crystallinity at 2θ values of 20.8°, 26.6°, and 59.9°. Specific authors are uncertain about quartz's effect on ceramics' strength. Boussouf et al. (2018) said that quartz impacts the material's strength. In contrast, alternative sources assert that quartz's mechanical strength is diminished due to immersion in β- to α-quartz at 573 °C throughout the cooling procedure. Quartz is composed primarily of silica, a ceramic brick constituent.

Starting from sample B100S0, the intensity of the muscovite ($Al_3HKO_{12}Si_3$) phase increased to sample B65S10. At 2θ = 40.1° and 51.0°, the muscovite (COD1100013) phase exhibits a high degree of crystallinity. As (Rodrguez-Navarro et al. (2003) stated, Muscovite decomposes into mullite when exposed to elevated temperatures. Muscovite initiates dihydroxylation at temperatures exceeding 900 °C, followed by partial melting and the formation of the mullite phase.

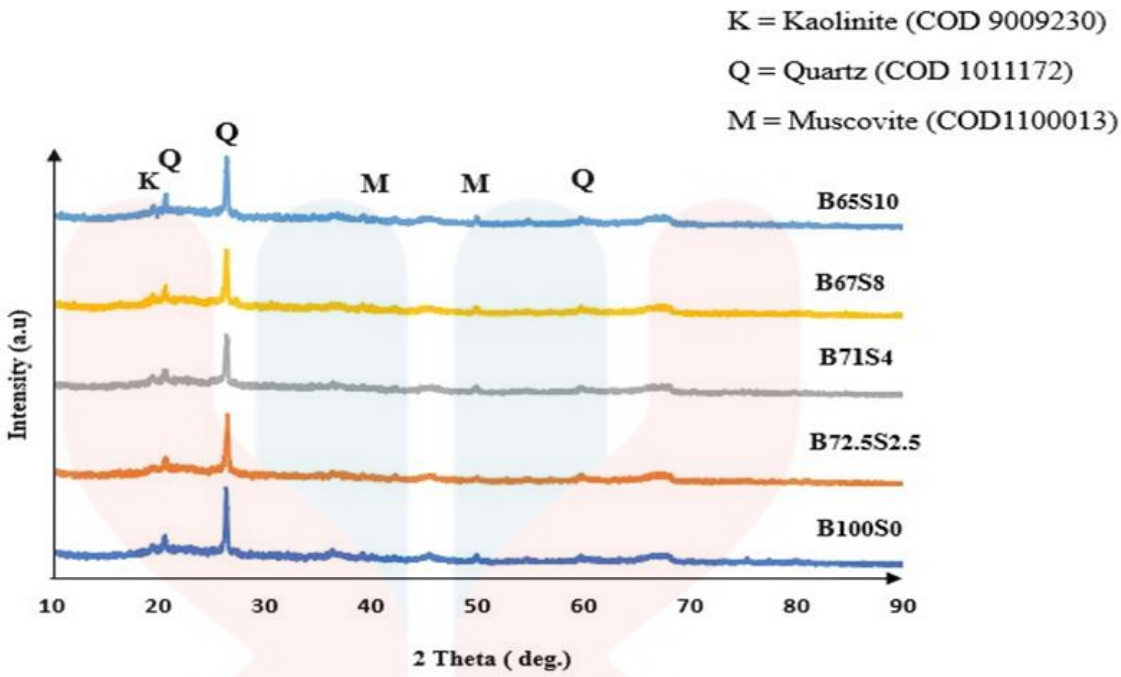

Figure 4.1: XRD pattern of different various of sample fired at 1000 °C.

The X-ray diffraction (XRD) patterns of B100S0, B72.5S2.5, B71S4, B67S8, and B65S10, which were fired at a temperature of 1100 °C, are illustrated in Figure 4.2. The outcomes above indicate that the phases present in the XRD analysis are quartz and mullite. The crystallinity of the sample pattern distribution exhibits an increase from 47.0% for sample B100S0 to 47.9% for sample B72.5S2.5, with sample B67S8 showing a slight decrease from 48.1% for sample B71S4 before rising to 44.9%. The sample B65S10 exhibits a marginal increase in crystallinity to 46.6%.

The mullite ($Al_4.8O_9.6Si.2$) phase exhibits a greater intensity in sample B65S10 than in sample B100S0. The mullite phase (COD 7105575) shows a strong crystallinity at 2θ values of 16.4°, 39.1°, 40.8°, and 60.5°. The low intensity of mullite ($Al_4.8O_9.6Si.2$) was determined to result from its recent formation and incomplete crystallisation. According to (Meng et al. (2016), the mullite phase was generated due to the degradation of the kaolinite phases throughout the sintering procedure. According to the findings, defects such as dislocations and lattice holes might have been present in the low intensity mullite phase that was generated. The quartz and mullite diffraction

peaks were identified as the principal constituent phases in the fired ceramic bodies, which are held together by the produced glassy phase, as stated by (Dong et al. (2017). As the firing temperature increases, fluxing compounds undergo diffusion into the disintegrating clay. Following this, they react in a manner that produces mullite crystals. Mullite, an essential crystal, contributes significantly to the mechanical integrity of ceramics (Ngayakamo et al., 2019). Ceramics physical and mechanical properties were improved by the development of mullite crystals and a glassy phase.

Sample B100S0 exhibited an increase in quartz (SiO2) intensity, which subsequently declined at B72.5S2.5 before rising again at B65S10. The quartz phase (COD 1011172) shows a high degree of crystallinity which is 46.6 % at $2\theta = 26.6°$ and 59.9°. The quartz-like structures show a crystalline distribution peak due to the phase transition during the heating procedure. The observed peak corresponds to the results of a study by (Zhang et al. (2008), which determined that the phase with the highest intensity (COD 1011172) is quartz ($\theta = 26.6°$). The study demonstrated that the amorphous XRD pattern of SiO_2 remained amorphous at 53.4 % despite undergoing sintered treatment at 800 °C. Before the design crystallises, it must be sintered at temperatures between 1000 and 1600 °C. Even though some of the samples in this investigation showed a semicrystalline structure after fired at 1000 and 1000 °C, this didn't apply to all of them. As the results derived from the samples at 1100 °C showed, crystallisation had been initiated, but the material was not yet crystalline.

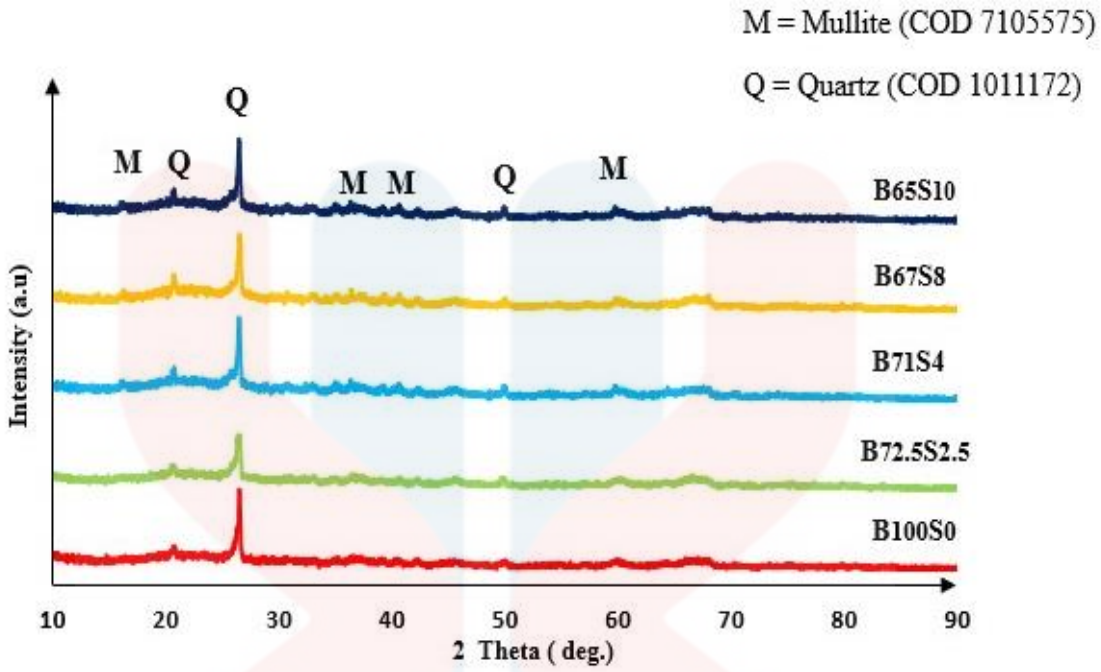

Figure 4.2: XRD pattern of different various of sample fired at 1100 °C.

4.2 Fourier Transform Infrared Spectroscopy (FTIR)

The FTIR analysis of the ceramic brick samples B100S0, B72.5S2.5, B71S4, B67S8, and B65S10 were fired at temperatures of 1000 °C and 1100 °C is illustrated in Figure 4.3. This characterization was performed to examine the chemical bonding and the presence of mineralogical phases. The focus of this investigation was FTIR analysis in the mid-IR spectrum. Single bond region (2500-4000 cm^{-1}), triple bond region (2000-2500 cm^{-1}), double bond region (1500-2000 cm^{-1}), and fingerprint region (600-1500 cm^{-1}) are the four regions that make up the mid-IR spectrum. As shown in the results above, the highest peaks formed at 1000 °C in B100S0, B72.5S2.5, B71S4, B67S8, and B65S10 are 1054.25 cm^{-1}, 1058.28 cm^{-1}, 1057.87 cm^{-1}, 10577.35 cm^{-1}, and 1061.15 cm^{-1}, respectively. At 1100 °C, the highest peaks are 1054.19 cm^{-1}, 1061.32 cm^{-1}, 1057.96 cm^{-1}, 1054.23 cm^{-1}, and 1058.66 cm^{-1}.

The peaks observed at a temperature of 1000 °C are as follows: 1054.25 cm^{-1}, 1058.28 cm^{-1}, 1057.87 cm^{-1}, 10577.35 cm^{-1}, and 1061.15 cm^{-1}. At 1100 °C, the peaks are as follows, 1054.19 cm^{-1}, 1061.32 cm^{-1}, 1057.96 cm^{-1}, 1054.23 cm^{-1}, and 1058.66 cm^{-1}. These values correspond to vibrations associated with Si-O stretching in silicate compounds commonly encountered in ceramics and clay minerals like kaolin and ball clay. Bohara et al. (2018) report that the bending absorptions of OH and stretching and bending absorptions of Si–O occur in the FTIR bands corresponding to clay minerals, spanning the range of 1300 to 400 cm^{-1}. Multiple distinct, robust bands are generated by the Si–O stretching vibrations of clay minerals within the 1100–1000 cm^{-1} range. Using FTIR absorption peaks at 1054.25 cm^{-1}, 1058.28 cm^{-1}, 1057.87 cm^{-1}, 1057.35 cm^{-1}, and 1061.15 cm^{-1}, the Si–O vibrations of the tetrahedral sheet of the fired brick sample's raw minerals were identified at 1000 °C. At 1100 °C, the Si–O vibrations of amorphous silica as proven by the outcomes, the peaks decreased towards higher wavenumbers.

This leads to the conclusion that the presence of ball clay and kaolin clay in the samples results in the formation of silicate compounds. The Si-O bonds within these tetrahedra are vital for the stability and integrity of the clay minerals. Si-O relationships are a constituent of the overall matrix of the ceramic material. The strength and rigidity of the ceramic matrix are derived from the network formed by the arrangement of oxygen and silicon atoms. The ceramic bricks become more robust as the firing temperature rises from 1000 °C to 1100 °C, making the material denser (Bohara et al., 2018).

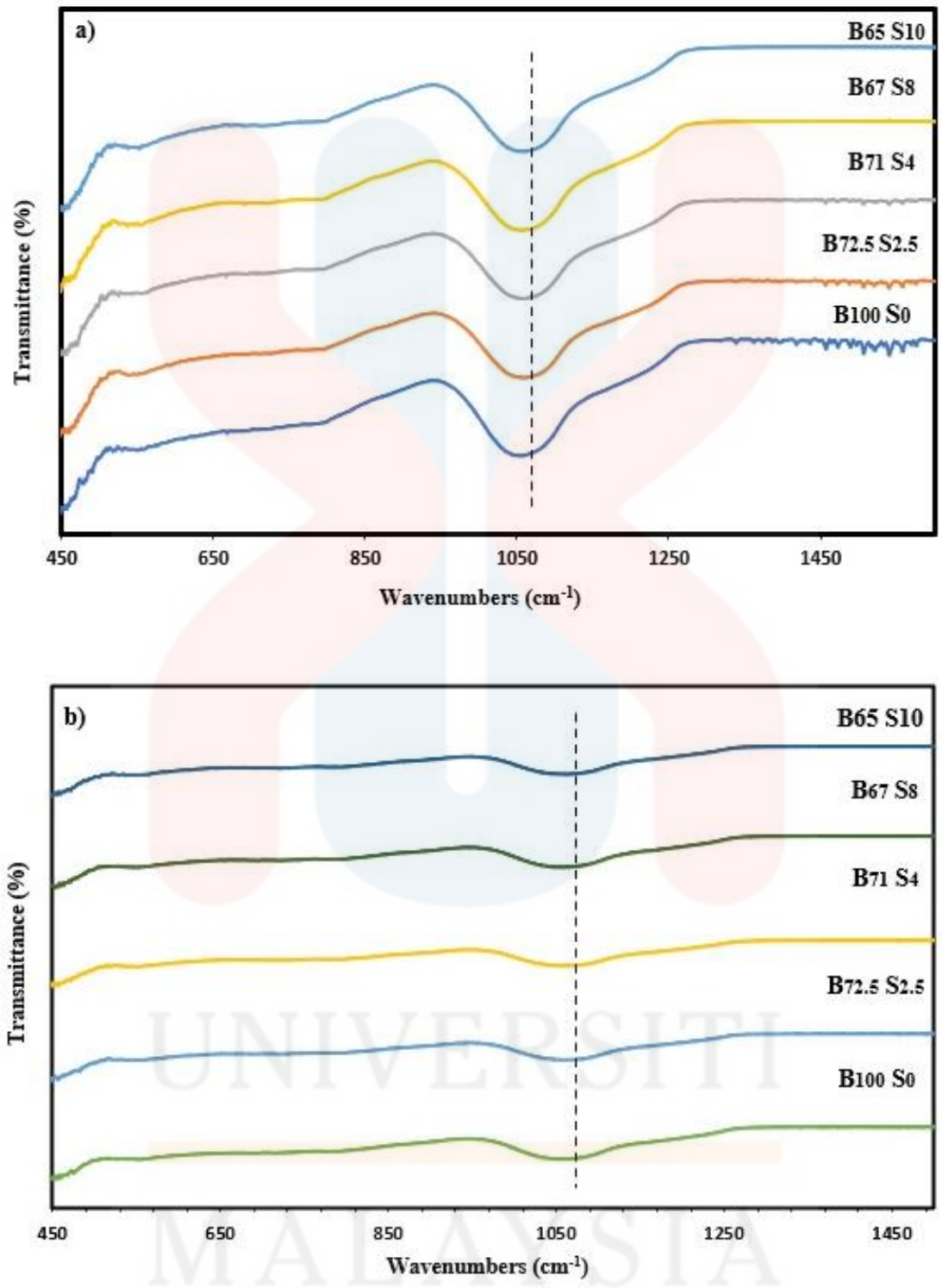

Figure 4.3: FTIR spectra of different various of sample fired at a) 1000 °C and b) 1100 °C.

4.3 Thermogravimetric Analysis (TGA)

As illustrated in Figure 4.4, the thermogravimetric analysis (TGA) spectrum of a ball clay sample heated in an air atmosphere at a rate of 10.00 °C min^{-1}. The initial weight loss of approximately 3.1% at 41.52 °C, when the samples began to lose weight, and the final weight loss of 284.13 °C, where the samples ceased to lose weight, was due to the dehydration of physically absorbed water on the crystal surface and water molecules surrounding the silicate layer. The process of organic substance degradation transpired during which the substances underwent complete decomposition at high temperatures ranging from 700 to 1000 °C, resulting in a weight loss of approximately 10.4 %. (Xi et al. 2005) & Lena et al. 2012).

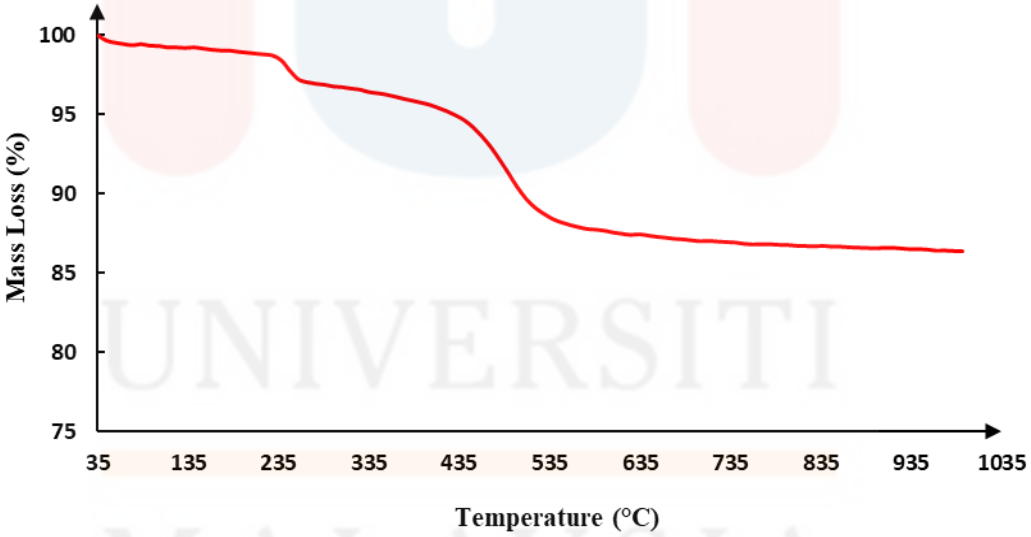

Figure 4.4: TGA spectrum of ball clay.

The thermogravimetric analysis (TGA) results for kaolin clay in Figure 4.5 illustrated the weight loss resulting from dehydration and dehydroxylation as the heating temperature increased. The sample experiences its initial weight loss of 6.0332 % at 72.01 °C and concludes with a weight loss of 553.39 °C. Given that the heating process was conducted in an air atmosphere at a rate of 10.0 °C min^{-1}, the mass loss of water absorbed, structurally associated water, and OH groups expelled from the mineral sample are all included in the weight loss. Based on the analysis of the TG curves and the obtained results, it was approximated that 90% of the clay samples contained kaolinite minerals. The matching TGA peak, which typically occurs between 400 °C and 600 °C, is due to the dehydroxylation of the mineral kaolinite. 6.0% of the weight of pure kaolinite is lost when heated to these temperatures (Faqir et al. 2018).

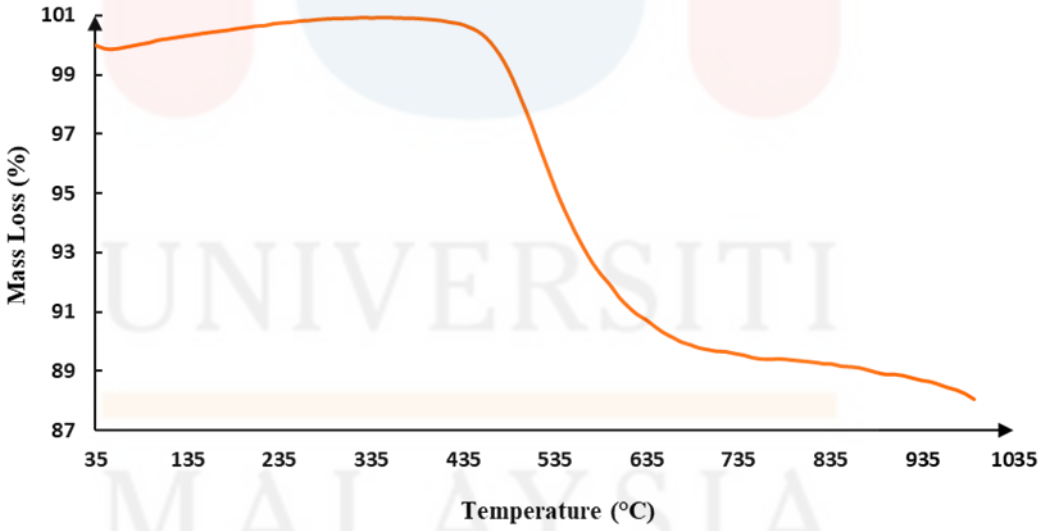

Figure 4.5: TGA spectrum of kaolin clay.

The weight of loss incurred by the sawdust sample during thermogravimetric analysis (TGA) was illustrated in Figure 4.6. Raw sawdust undergoes thermal degradation in three distinct phases. Between 65 °C and 100 °C, the initial stage transpires at 10.00 °C min^{-1} in the air atmosphere. The minor weight reduction observed in this phase is likely attributable to residual moisture desorption. An estimated 200–392 °C is utilised for the second phase. It illustrates a substantial reduction in body weight of 57 %. The possible cause for this is hemicellulose decomposition (Gonzalez-Serrano et al., 2004). The third phase was visible in the TG curve between 392 and 400 °C. This phenomenon is explained by lignin and cellulose degradation into carbonyl, lactone, and carboxyl groups. The potential cause could be the desorption of CO_2 and CO from cellulose, which converts it into volatile organic compounds in sawdust. As depicted in Figure 4.6, the carbonisation process was complete when the temperature reached 400 °C, at this point, no significant weight loss occurred. Consequently, sawdust carbonisation occurred at a temperature of 400 °C (Shrestha et al., 2019).

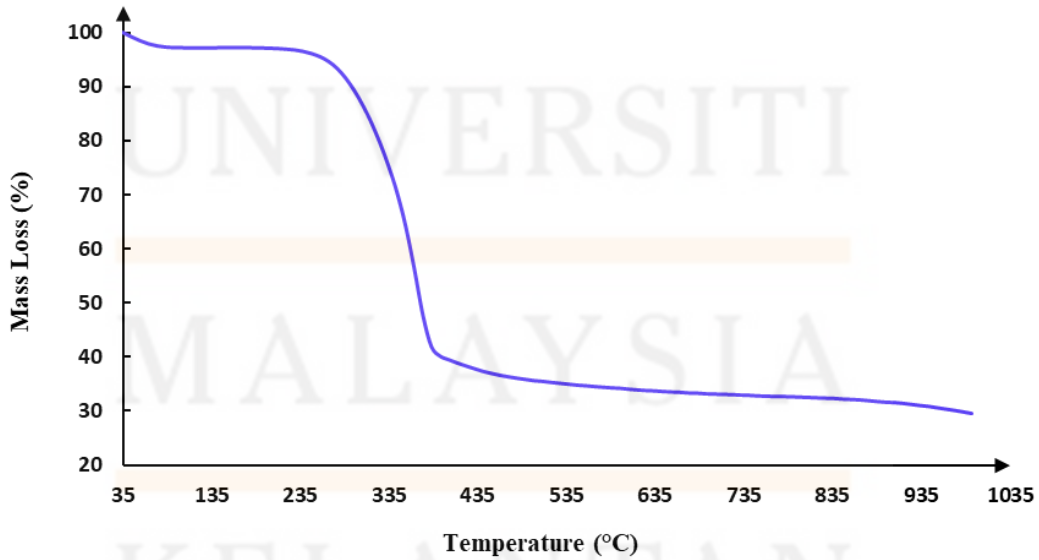

Figure 4.6: TGA spectrum of sawdust.

The thermogravimetric analyses (TGA) of several samples, namely B100S0, B72.5S2.5, B71S4, B67S8, and B65S10, which were heated at a rate of 10.00 °C min^{-1} in ambient air, are depicted in Figure 4.7. The above results indicate the formation of three distinct phases. In brick production, water evaporation, carbonate decomposition, and added sawdust combustion are the primary causes of weight loss. The initial stage consists of dehydrating the interlayer and physically absorbing water from the ceramic at temperatures between 100 and 250 °C (Drebushchak et al., 2010) or 100 to 350 °C. This is followed by dehydroxylation, which resembles structural hydrolysis and typically occurs at high temperatures (Shoval et al., 2013). Frequently found in ceramic bricks are clay minerals, which are hydrous aluminium silicate minerals. Kaolinite, illite, and montmorillonite are all prevalent clay minerals. The hydroxyl groups comprising these minerals' structures are bonded to the crystal lattice through chemical bonds. As the temperature rises during TGA, the thermal energy applied to the ceramic brick initiates various reactions.

Dehydroxylation entails the elimination of hydroxyl groups from clay minerals, resulting in the emission of water vapour as a gas and a discernible reduction in weight as indicated by the thermogravimetric analysis curve (Derkowski and Artur Kuligiewicz, 2022). Clay mineral dehydroxylation is a critical process between 500 and 900 degrees Celsius. The temperature range of 600-900 °C is where carbonate decomposition occurs, with carbon dioxide emission starting at 650 °C and concluding between 800 and 850 °C. Ceramic minerals undergo crystalline lattice destruction and the formation of new phases, including gehlenite, diopside, anorthite, mullite, and hematite, between 900 and 1000 °C (Solongo et al. 2020). The mass loss for all samples

occurs at 900 °C; consequently, the optimal firing temperature for ceramic bricks is approximately 900 °C, with temperatures exceeding 900 °C being optimal.

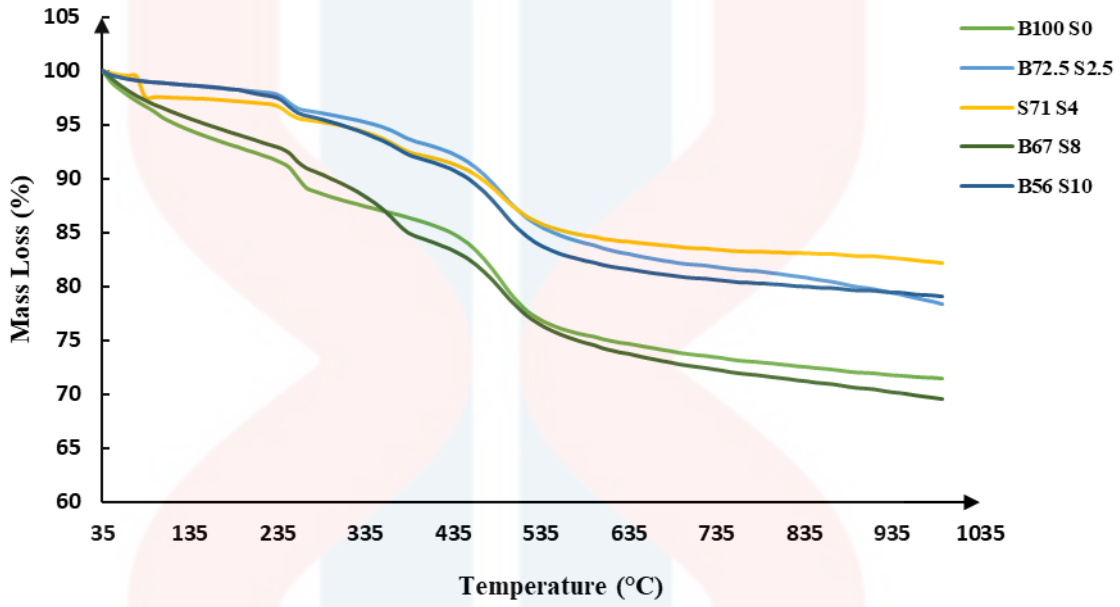

Figure 4.7: TGA spectrum for various sample.

4.4 Physical Properties of Ceramic Brick

4.4.1 Density

Figure 4.8 shows the various density value of different samples at 900 °C of firing temperature. At 900 °C, the highest density value is 1.821 g/cm^3 at B100S0 sample compared to others. The value starts to reduce from B72.5S2.5, B71S4, B67S8 and B65S10 where at B72.5S2.5 the density value is 1.652 g/cm^3, B71S4 is about 1.607g/cm^3, at B67S8 the density is 1.428 g/cm^3 and finally for the B65S10 is 1.403 g/cm^3.

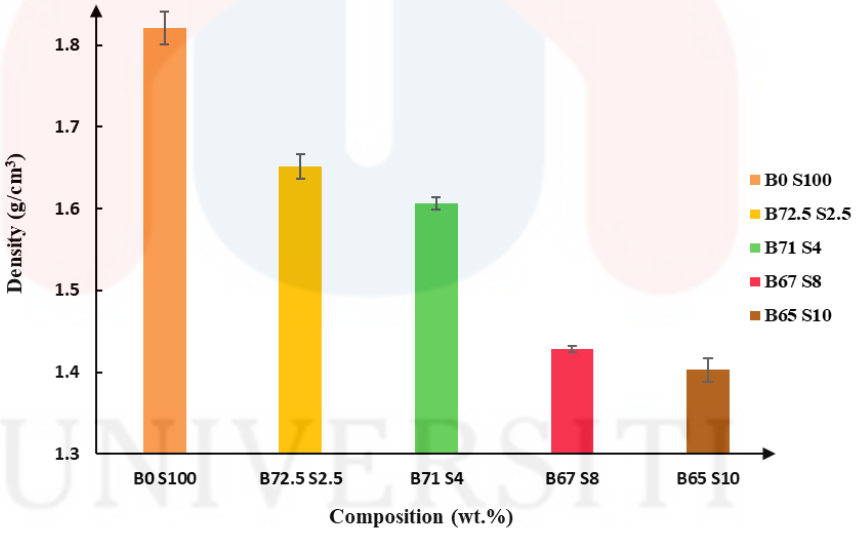

Figure 4.8: Density values of various sample fired at 900 °C.

At temperature of 1000 °C, the value of density is 1.851 g/cm^3 at sample B100S0 where the highest among others. The density decreased with increase of sawdust in ceramic brick where at B72.5S2.5 the density is 1.658 g/cm^3, B71S4 is about 1.615 g/cm^3, at B67S8 the density is 1.488 g/cm^3 and the last one at B65S10 the density is 1.456 g/cm^3 as shown in Figure 4.9.

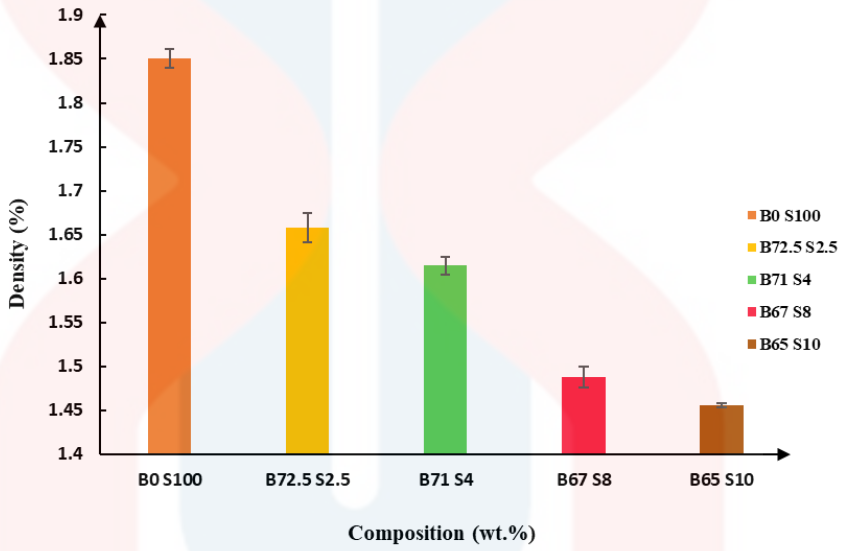

Figure 4.9: Density values of various sample fired at 1000 °C.

For the 1100 °C temperature, the density value is the highest compared to 900 °C and 1000 °C as shown in Figure 4.10. At B100S0 the density is 1.901g/cm^3, at B72.5S2.5 it started to increase at 1.697 g/cm^3 compared to 900 °C and 1000 °C. At B71S4 density value is 1.653 g/cm^3, B67S8 around 1.599 g/cm^3 and at the B65S10 its about 1.592 g/cm^3. The value of density decreased at the highest wt.% of sawdust.

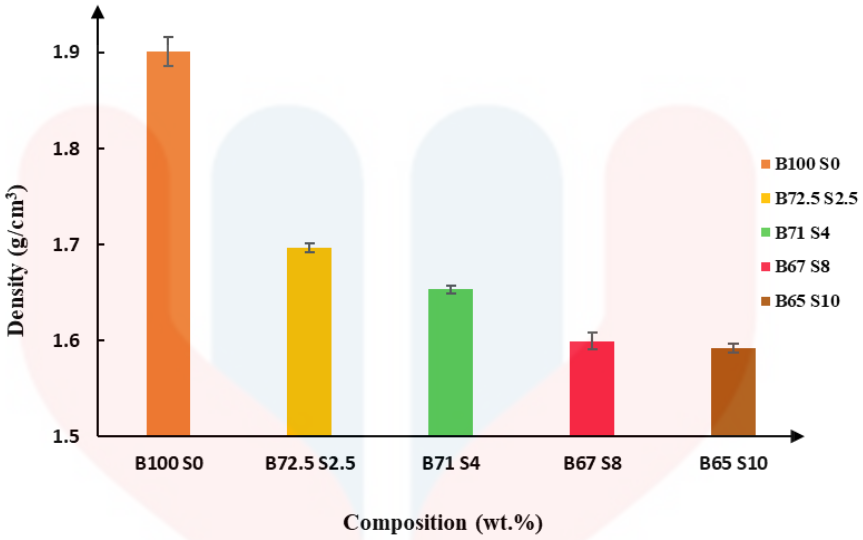

Figure 4.10: Density values of various sample fired at 1100 °C.

This can be deduced that the density of the ceramic brick decreases with the addition of sawdust. The observed behaviour has been ascribed to the formation of specific pores within the clay structure during the incineration of sawdust waste. However, it is important to note that the density of the ceramic brick is most excellent at a firing temperature of 1100 °C, as compared to 900 °C and 1000 °C. Additionally, the increased density value indicates that the high-temperature firing procedure successfully eliminated the porosity. Elevated firing temperature results in the filling of pores with the glassy phases generated (Olgun et al. 2005). This demonstrates a significant increase in ceramic density by adding 2.5 wt.% sawdust to the 1100 °C firing process. A correlation exists between the water absorption capacity and durability of clay bricks and their density. A higher volume density of clay blocks corresponds to greater robustness and reduced water absorption (Phonphuak., 2020).

4.4.2 Porosity

Figure 4.11 shows the apparent porosity of various wt.% of sawdust at firing temperature of 900 °C. The trend for the apparent porosity at 900 °C is increased as the addition of sawdust increased. Based on the figure, the value of apparent porosity for the B100S0 is 41.95 %, B72.5S2.5 where the apparent porosity is 42.06 %, B71S4 is about 42.26 %, at B67S8 is 42.37 % and for the highest amount of apparent porosity is at B65S10 where 43.11 %.

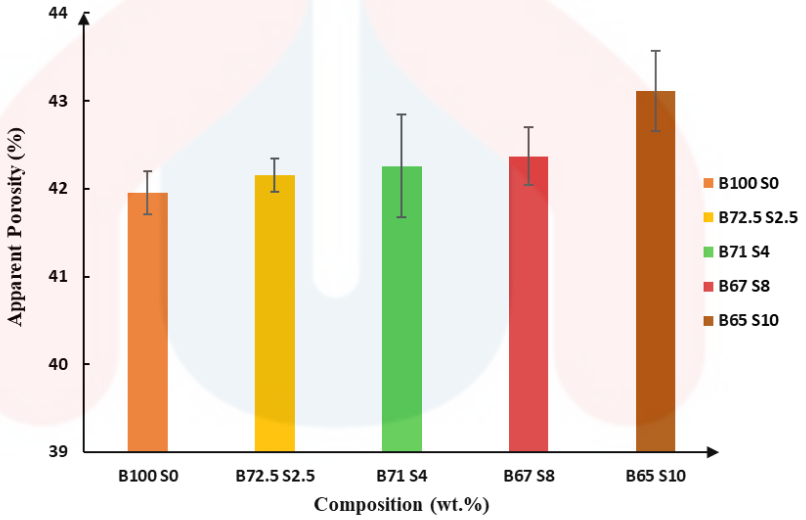

Figure 4.11: Apparent porosity of various sample fired at 900 °C.

Based on the Figure 4.12, at 1000 °C firing temperature the apparent porosity starts to decease slightly compared to 900 °C because of the firing temperature that increased. At B100S0 the value of apparent porosity is 40.7 % and increased as the addition of sawdust increases. For B72.5S2.5 the apparent porosity is 41.22 %, at B71S4 the value is 41.3 %, at B67S8 the apparent porosity is 42.23 and at B65S10 the apparent porosity is the highest among other samples which is 42.58 %.

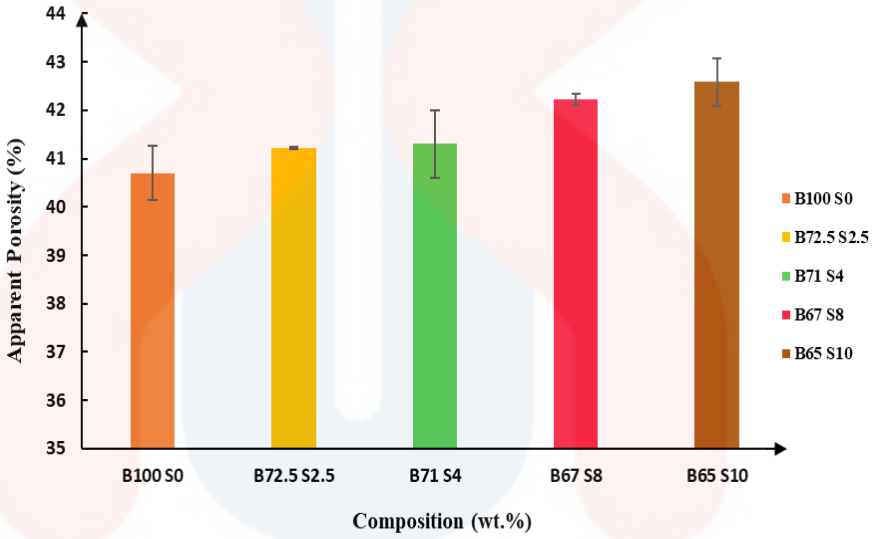

Figure 4.12: Apparent porosity of various sample fired at 1000 °C.

For the 1100 °C of firing temperature the apparent porosity starts to reduce compared to 900 °C and 1000 °C temperatures. Figure 4.13 shows the various samples where at B100S0 the apparent porosity is 38.06% followed by B72.5S2.5 the value is 38.18%, at B71S4 the value is 38.37% and it continue to increase by 38.73 % at B67S8 and the last one for B65S10 where the highest amount of sawdust in ceramic brick, the apparent porosity is 39.37% respectively.

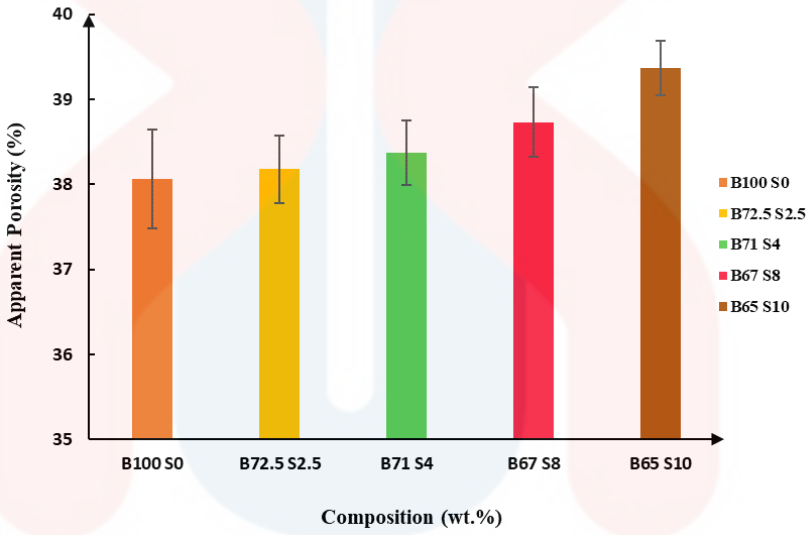

Figure 4.13: Apparent porosity of various sample fired at 1100 °C

The B65S10 specimen with a porosity of approximately 42.58% was produced by incorporating 10 wt.% sawdust after being fired at 900 °C, as illustrated in Figure 4.13. As shown in Figure 4.13, the bricks B72.5S2.5 containing 2.5% sawdust fired at 1100 °C exhibited the lowest porosity of 38.18%. Thus, the introduction of sawdust waste into fired clay bricks resulted in porosity, which was eliminated during the firing process. Consequently, increased sawdust waste incorporated into clay bricks leads to a corresponding rise in open porosity, resulting in clay bricks with greater porosity (Phonphuak, 2020). The apparent porosity value is at its minimum at 1100 °C during

firing due to forming a glassy phase in the ceramic brick during vitrification. This process induces densification and subsequent reduction in porosity in the ceramic brick (Olgun et al. 2005).

4.4.3 Water Absorption

Figure 4.14 shows the water absorption of various sample fired at 900 °C. The highest % of water absorption is at B65S10 which are 44.54 % where it shown that an increasing of water absorption value as the sawdust increases. At B100S0 the % water absorption is 32.66 %, at B72.5S2.5 the value is 34.77 % followed by B71S4 the value of the water absorption is 35.57 % and the last one for the B67S8 sample the value of the water absorption is 41.99 %.

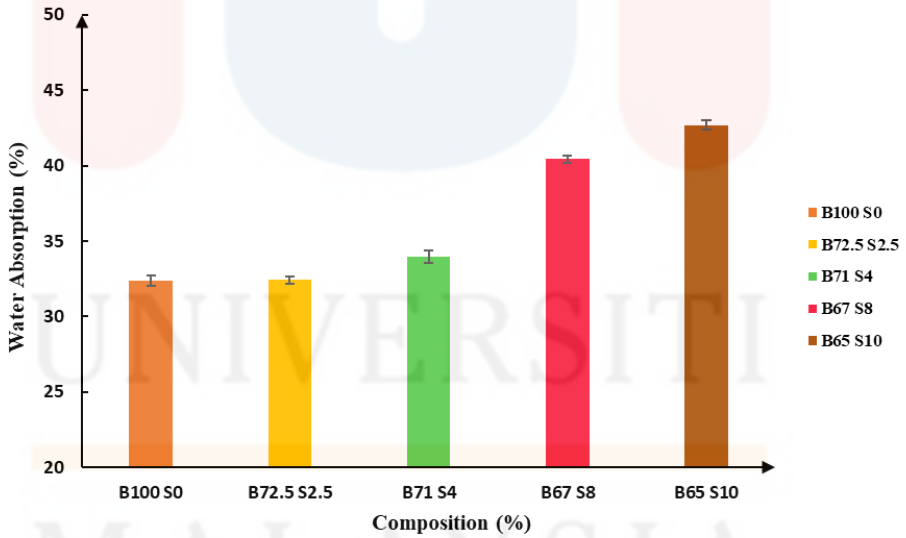

Figure 4.14: Water absorption of various sample fired at 900 °C.

Based on the Figure 4.15, shows the % of water absorption for 1000 °C temperature of various sample. The results shows that the % of water absorption increases too as in 900 °C when the sawdust addition is increases. At B100S0 the % of water absorption is 32.37% followed by B72.5S2.5 the value of the water absorption is 32.41 %, at B71S4 the value is 33.95 %. At B67S8 the water absorption is 40.43 % and the highest % of water absorption is 42.68 % at B65S10 as the sawdust of addition increases in ceramic brick.

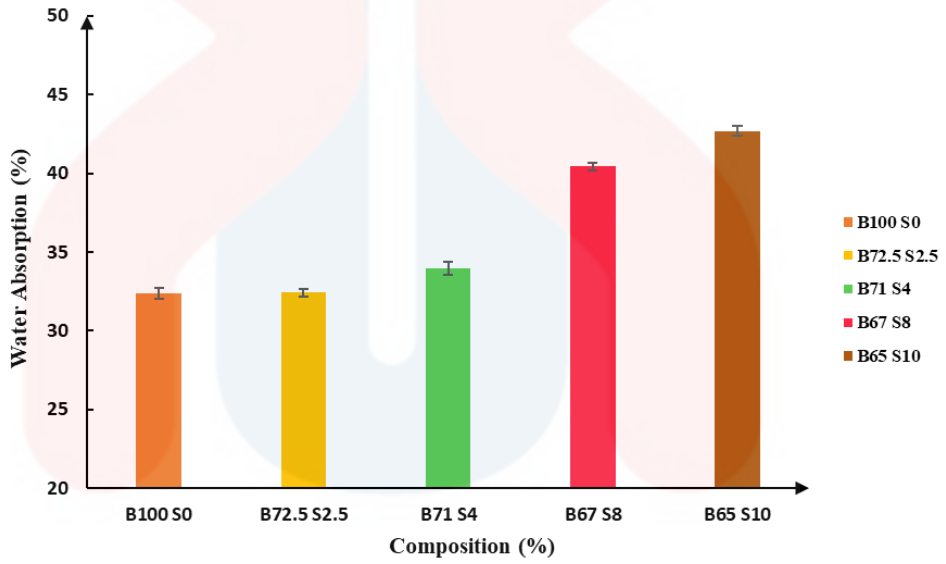

Figure 4.15: Water absorption of various sample fired at 1000 °C.

For the 1100 °C of firing temperature, the % of water absorption starts to reduce compared to 900 °C and 1000 °C. Based on the Figure 4.16 shown, at B100S0 the value of water absorption is 25.26 % followed by B72.5S2.5 the value is 28.69 %, at B71S4 the % of water absorption is 30.34 %, at B67S8 the value of water absorption is 31.8 % and the highest % of water absorption is 32.69 % as the sawdust increases at B65S10.

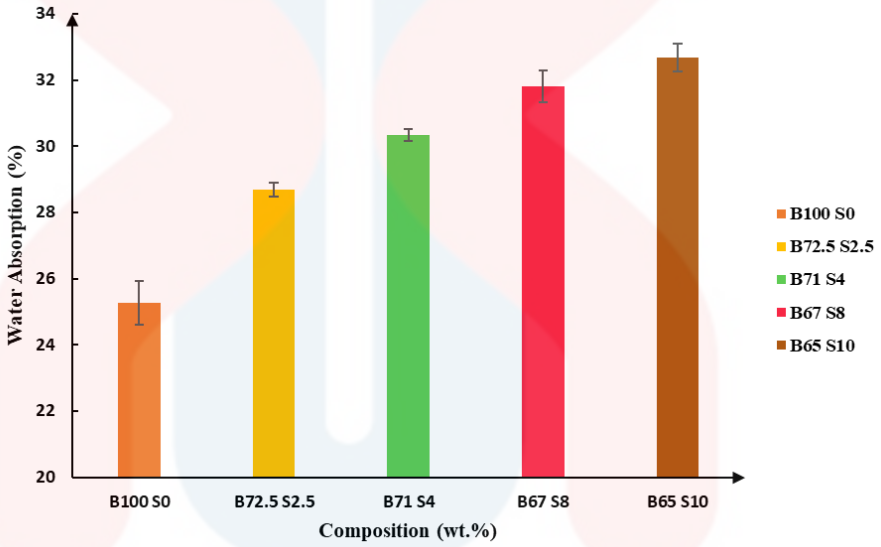

Figure 4.16: Water absorption of various sample fired at 1100 °C.

The percentage of water absorption in ceramic brick increases as the amount of added sawdust rises, as indicated by the above results. The sample B65S10, fired at 900 °C, exhibited the highest water absorption percentage of 44.54%, as shown in Figure 4.14. Conversely, sample B72.5S2.5, fired at a high temperature of 1100 °C, demonstrated the lowest water absorption percentage of 28.69 %. Increased water absorption percentage indicates a greater quantity of pores in the sample. Clay bricks' water absorption is correlated with their durability. Water absorption can eventually diminish the durability of clay brick. Density is an essential condition to reduce water

absorption within the brick body. A detrimental relationship was observed between the increase in firing temperature and the strength of the clay bricks, specifically in terms of water absorption. An increase in compressive strength and a decrease in the water absorption rate in the brick structure. Phonphuak (2020) says that porosity impacts support water absorption outcomes. The glassy phase is augmented, and the open pores in ceramic bricks are sealed due to the elevated firing temperature of 1100 °C. It was established through the water absorption test that the water absorption of porous ceramic is influenced by its porosity. Therefore, an increase in the quantity of by-product leads to a corresponding rise in water absorption (Demir, 2008).

4.5 Mechanical Properties of Ceramic Brick

4.5.1 Compressive Strength Test

Figure 4.17 shows the compressive strength of various sample fired at 900 °C. The highest compressive strength between the addition of sawdust is 7.21 MPa at B72.5S2.5 compared to 7.3 MPa at B100S0 followed by 6.84 MPa at B71S4. At B67S8 the compressive strength is 6.4 MPa and at the B65S10 the value decreased to 6.3 wt.% respectively. This result indicates that the compressive strength of ceramic bricks decreases as the amount of sawdust added increases.

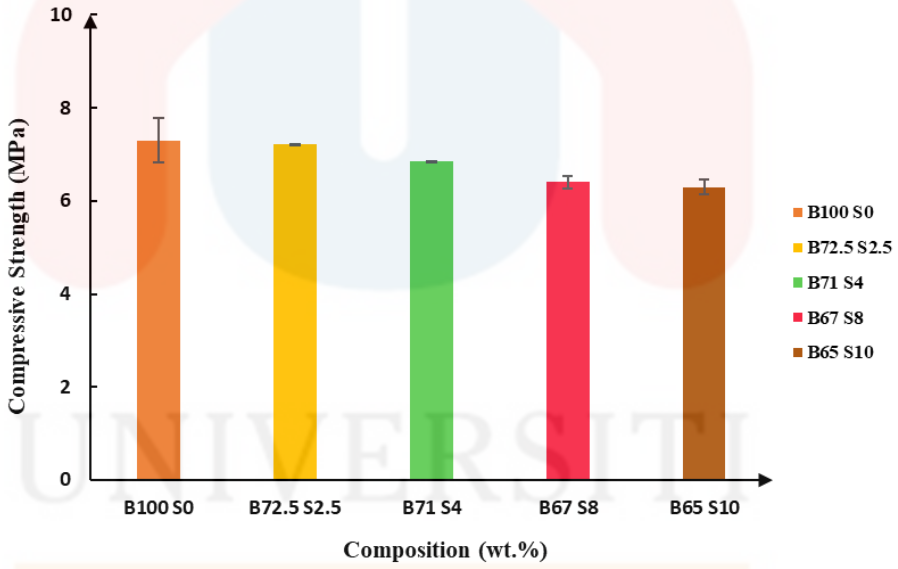

Figure 4.17: Compressive strength of various sample fired at 900 °C.

Based on the Figure 4.18 shows the compressive strength of various sample fired at 1000 °C. Based on the results, at B100S0 % the value of the compressive strength is 8.3 MPa where the trend increases from 900 °C. The highest compressive strength value is 8.0 MPa at B72.5S2.5 and at B71S4 the value is 7.7 MPa. At B67S8 the compressive strength is 7.6 MPa and the last at B65S10, the value is 7.4 MPa where the compressive strength is decreased.

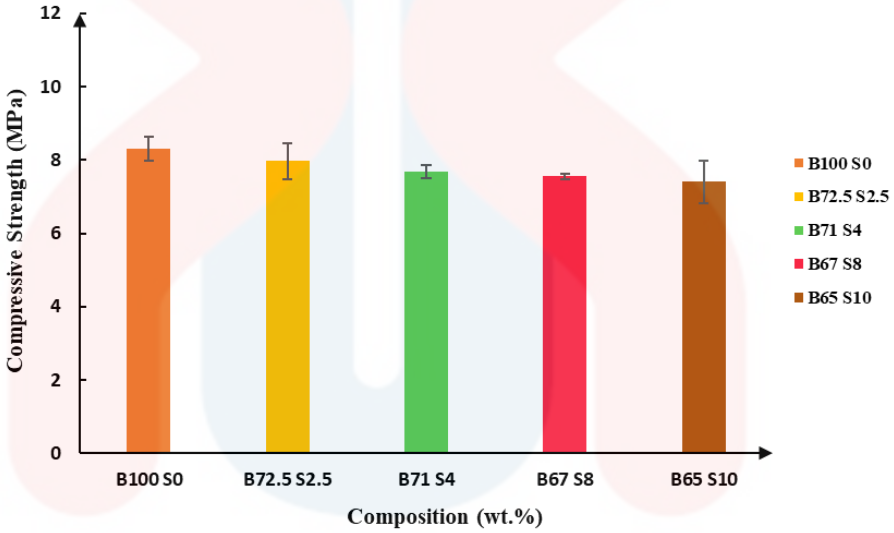

Figure 4.18: Compressive strength of various sample fired at 1000 °C.

At 1100 °C of firing temperature, the compressive strength is the highest compared to 900 °C and 1000 °C. At B100S0 the compressive strength is 17.26 MPa followed by 16.87 MPa at B72.5S2.5 and at B71S4 the value is 13.83 MPa. At B67S8 the value is 13.75 MPa and decreased to 12.80 MPa at B65S10 when the addition of sawdust increases.

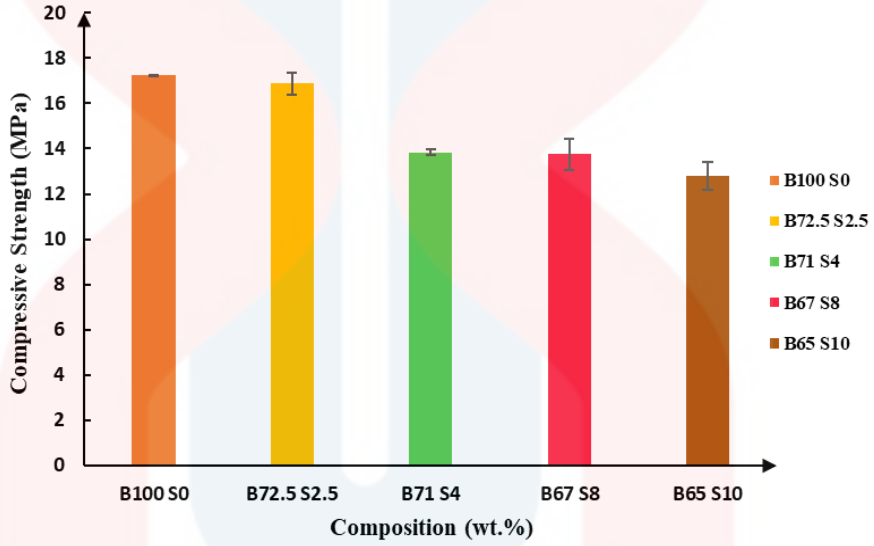

Figure 4.19: Compressive strength of various sample fired at 1100°C.

From the results above, it can be observed that increasing the amount of sawdust added to ceramic brick reduces its strength. As shown in Figure 4.19, the B72.5S2.5 with the highest compressive strength of 16.87 MPa was fired at 1100 °C. The B65S10 with the lowest compressive strength was fired at a high temperature of 900 °C. According to the findings of the research (Bánhidi et al., 2008), an increase in the quantity of sawdust waste utilised resulted in a decrease in the compressive strength of the clay bricks. This can be attributed to the increase in porosity and reduction in density. An increase in firing temperature results in an enhancement of the compressive

strength due to the concomitant increase in density and decrease in porosity. Firing heat between 1000 °C and 1100 °C to clay bricks substantially increases their compressive strength. The compressive strength values of the samples containing sawdust waste in proportions varying from 2.5 % to 10 % by weight ranged from 6.3 to 16.87 MPa (Phonphuak., 2020). The compressive strength is influenced by ceramics' additive content and porosity properties (Beal et al., 2019). The reduced density of the material and the larger pores in ceramic brick contributed to its low mechanical strength. Therefore, mechanical strength decreases with increasing porosity dispersion. Compressive strength is influenced by the porosity fraction of porous ceramic as porosity increases, strength decreases (Sylvain Meille et al., 2012).

4.6 Relationship between composition, physical and mechanical properties

Based on the results obtained using various compositions B100S0, B72.5S2.5, B71S4, B67S8, and B65S10, the physical and mechanical properties of ceramic bricks containing increasing amounts of sawdust 0, 2.5, 4, 8, and 10 wt. % by weight are determined. The density of ceramic bricks decreases with increasing sawdust content, as shown in Figures 4.8, 4.9, and 4.10. This phenomenon can be attributed to the formation of pores in the samples, which result from sawdust waste combustion (Phonphuak., 2020). As shown in Figures 4.11, 4.12, and 4.13, the porosity rises with the addition of sawdust. Phonphuak (2020) provides evidence that an increase in the quantity of sawdust waste incorporated into clay bricks leads to a corresponding rise in open porosity, resulting in clay bricks with greater porosity. In addition, the water absorption of ceramic bricks increases with the addition of sawdust, as illustrated in Figures 4.14, 4.15, and 4.16, because the increased pore count contributes to the water absorption. As shown in Figures 4.17, 4.18, and 4.19, the compressive strength of the ceramic brick

decreases with increasing sawdust content. This is because ceramic brick has a low density, high porosity, and high-water absorption.

Nevertheless, the ceramic brick's compressive strength increased as the firing temperature increased. This can be attributed to the brick's reduced in water absorption, increased density, and complete combustion of the sawdust at elevated temperatures. In this investigation, firing clay bricks between 1000 and 1100 °C significantly increases their compressive strength.

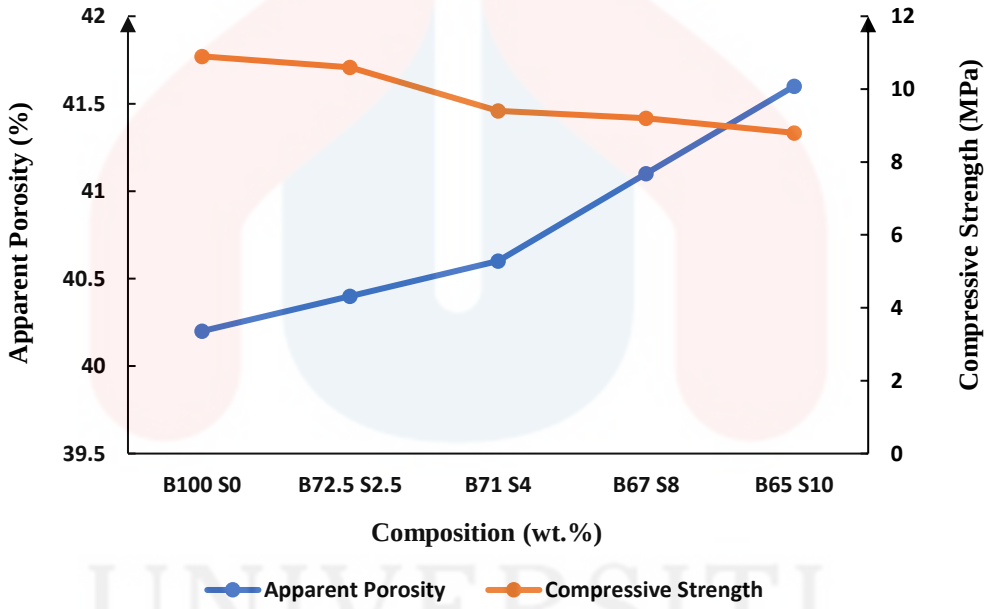

Figure 4.20: The relationship between apparent porosity (%) and compressive strength (MPa) fired at 900 °C,1000 °C and 1100 °C.

CHAPTER 5

CONCLUSION AND RECOMMENDATIONS

5.1 Conclusion

This research investigates ceramic bricks physical and mechanical characteristics using different raw materials, including sawdust, kaolin clay, and ball clay, as additives. The study also assesses the impact of sawdust addition. The effect of firing ceramic bricks with varying compositions at 900 °C, 1000 °C, and 1100 °C on their physical and mechanical properties was determined. Based on the findings, it can be inferred that the addition of sawdust to ceramic bricks results in a reduction in density, an increase in porosity and water absorption, and a subsequent decrease in compressive strength due to the increased pore production within the brick. Nevertheless, this study provides evidence that increasing the firing temperature increased compressive strength, more significant densification, reduced porosity, and water absorption in the ceramic brick.

5.2 Recommendation

The physical and mechanical properties of the ceramic brick can be enhanced by varying some factors. The recommendations are:

a) Increase the firing to temperature to 1200 ℃ as stated by (Johari et al. (2010) to observe the porosity effects on the ceramic brick when fired at more higher temperatures compared to 900 °C, 1000 °C and 1100 °C.

b) The ceramic brick must undergo Scanning Electron Microscopy (SEM) where observe the morphology in cross sectional. The sample's surface morphology, including its grain structure, grain boundaries, and pore structure, can be observed by using a Scanning Electron Microscopy (SEM), which has a high magnification of up to 30,000 times and can be employed.

c) The ceramic brick must undergo hardness test to enhance the mechanical properties. The hardness of ceramic sample can be determined by using Vickers hardness test.

REFERENCES

Ahmed, W., Khushnood, R. A., Memon, S. A., Ahmad, S., Baloch, W. L., & Usman, M. (2018). Effective use of sawdust for the production of eco-friendly and thermal-energy efficient normal weight and lightweight concretes with tailored fracture properties. *Journal of Cleaner Production*. https://agris.fao.org/agris-search/search.do?recordID=US201800139322

Ali, M. S., Ariff, A. H. M., Jaafar, C. N. A., Tahir, S. M., Mazlan, N., Maori, K. A., & Naser, H. (2017). Factors affecting the porosity and mechanical properties of porous ceramic composite materials.

Almssad, A., Almusaed, A., & Homod, R. Z. (2022). Masonry in the Context of Sustainable Buildings: A Review of the Brick Role in Architecture. *Sustainability*, *14*(22), 14734. https://doi.org/10.3390/su142214734

Bachir Chemani, & Halima Chemani. (2012). *Effect of Adding Sawdust on Mechanical-Physical Properties of Ceramic Bricks to Obtain Lightweight Building Material*. *6*(11), 2521–2525.

Bánhidi, V., & Gömze, L. A. (2008). Improvement of Insulation Properties of Conventional Brick Products. *Materials Science Forum*, *589*, 1–6. https://doi.org/10.4028/www.scientific.net/msf.589.1

Barbieri, L., Andreola, F., Lancellotti, I., & Taurino, R. (2013). Management of agricultural biomass wastes: Preliminary study on characterization and valorisation in clay matrix bricks. *Waste Management*, *33*(11), 2307–2315. https://doi.org/10.1016/j.wasman.2013.03.014

Barcenas, C. H., Delclos, G. L., El-Zein, R., Tortolero-Luna, G., Whitehead, L. W., & Spitz, M. R. (2005). Wood dust exposure and the association with lung cancer risk. *American journal of industrial medicine*, *47*(4), 349-357.

Beal, B., Selby, A., Atwater, C. G., James, C., Viens, C., & Almquist, C. B. (2019). A Comparison of Thermal and Mechanical Properties of Clay Bricks Prepared with Three Different Pore-Forming Additives: Vermiculite, Wood Ash, and Sawdust. *Environmental Progress & Sustainable Energy*, *38*(6). https://doi.org/10.1002/ep.13150

Bohara, N. B., Bhat, L. B., Ghale, D. B., Duwal, N., & Bhattarai, J. (2018). Investigation of the firing temperature effects on clay brick sample; Part-I: Mineralogical phase characterization. *BIBECHANA*, *16*, 122–130. https://doi.org/10.3126/bibechana.v16i0.21319

Bories, C., Borredon, M. E., Vedrenne, E., & Vilarem, G. (2014). Development of eco-friendly porous fired clay bricks using pore-forming agents: A review. Journal of environmental management, 143, 186-196.

Bose, S., & Das, C. (2014). Role of binder and preparation pressure in tubular ceramic membrane processing: design and optimization study using response surface methodology (RSM). Industrial & Engineering Chemistry Research, 53(31), 12319-12329

Boussouf, L., Fouzia Zehani, Youcef Khenioui, & N. Boutaoui. (2018). Effect of Amount and Size of Quartz on Mechanical and Dielectric Properties of Electrical Porcelain. *Transactions of the Indian Ceramic Society*, *77*(3), 132–137. https://doi.org/10.1080/0371750x.2018.1500148

Carty, W. M., & Senapati, U. (1998). Porcelain? Raw Materials, Processing, Phase Evolution, and Mechanical Behavior. *Journal of the American Ceramic Society*, *81*(1), 3–20. https://doi.org/10.1111/j.1151-2916.1998.tb02290.x

Chapagain, Y. P., Sapkota, S., Ghale, D. B., Bohara, N. B., Duwal, N., & Bhattarai, J. (2020). A case study on mineralogy and physico-mechanical properties of commercial bricks produced in Nepal. *SN Applied Sciences*, *2*(11). https://doi.org/10.1007/s42452-020-03535-y

Cotes-Palomino, M. T., Martínez-García, C., Eliche-Quesada, D., & Pérez-Villarejo, L. (2015). Production of Ceramic Material Using Wastes from Brewing Industry. *Key Engineering Materials*, *663*, 94–104. https://doi.org/10.4028/www.scientific.net/kem.663.94

Cultrone, G., Sebastián, E., Elert, K., de la Torre, M. J., Cazalla, O., & Rodriguez–Navarro, C. (2004). Influence of mineralogy and firing temperature on the porosity of bricks. *Journal of the European Ceramic Society*, *24*(3), 547–564. https://doi.org/10.1016/s0955-2219(03)00249-8

Daiana Lucía Simón, Nancy Esther Quaranta, Sebastián Emiliano Gass, Raul Ariel Procaccini, & Adrián Cristóbal. (2020). *Ceramic bricks containing Ni ions from contaminated biomass used as an adsorbent*. *30*(1). https://doi.org/10.1186/s42834-020-00067-3

Deac, T., Fechete-Tutunaru, L., & Gaspar, F. (2016). Environmental Impact of Sawdust Briquettes Use – Experimental Approach. *Energy Procedia*, *85*, 178–183. https://doi.org/10.1016/j.egypro.2015.12.324

Demir, I. (2008). Effect of organic residues addition on the technological properties of clay bricks. *Waste Management*, *28*(3), 622–627. https://doi.org/10.1016/j.wasman.2007.03.019

Derkowski, A., & Artur Kuligiewicz. (2022). Thermal Analysis and Thermal Reactions of Smectites: a Review of Methodology, Mechanisms, and Kinetics. *Clays and Clay Minerals*, *70*(6), 946–972. https://doi.org/10.1007/s42860-023-00222-y

DONG, W., BAO, Q., ZHOU, J., ZHAO, T., LIU, K., & HU, Z. (2017). Preparation of porcelain building tiles using "K_2O–Na_2O" feldspar flux as a modifier agent of low-temperature firing. *Journal of the Ceramic Society of Japan*, *125*(9), 690–694. https://doi.org/10.2109/jcersj2.16327

Drebushchak, V. A., Mylnikova, L. N., & Drebushchak, T. N. (2010). The mass-loss diagram for the ancient ceramics. *Journal of Thermal Analysis and Calorimetry*, *104*(2), 459–466. https://doi.org/10.1007/s10973-010-1230-x

Duggal, S. K. (2008). *Building materials*. New Age International.

Eliche-Quesada, D., Corpas-Iglesias, F. A., Pérez-Villarejo, L., & Iglesias-Godino, F. J. (2012a). Recycling of sawdust, spent earth from oil filtration, compost and marble residues for brick manufacturing. *Construction and Building Materials*, *34*, 275–284. https://doi.org/10.1016/j.conbuildmat.2012.02.079

Faqir, N. M., Reyad Shawabkeh, Al-Harthi, M. A., & Hamad Abdul Wahhab. (2018). Fabrication of Geopolymers from Untreated Kaolin Clay for Construction Purposes. *Geotechnical and Geological Engineering*, *37*(1), 129–137. https://doi.org/10.1007/s10706-018-0597-5

Farazela, M., Arib, M., Muhamad Azmi, M., Shazmin Aniza, A., & Azhan, A. (2021). Compressive Strength Performance of Composite Sand Cement Brick with Power Saw Wood. *Journal of Physics: Conference Series*, *2051*(1), 012050. https://doi.org/10.1088/1742-6596/2051/1/012050

Farnood Ahmadi, P., Ardeshir, A., Ramezanianpour, A. M., & Bayat, H. (2018). Characteristics of heat insulating clay bricks made from zeolite, waste steel slag and expanded perlite. *Ceramics International*, *44*(7), 7588–7598. https://doi.org/10.1016/j.ceramint.2018.01.175

Horisawa, S., Sunagawa, M., Tamai, Y., Matsuoka, Y., Miura, T., & Terazawa, M. (1999). Biodegradation of nonlignocellulosic substances II: physical and chemical properties of sawdust before and after use as artificial soil. *Journal of Wood Science*, *45*(6), 492–497. https://doi.org/10.1007/bf00538959

Humans, I. W. G. on the E. of C. R. to. (2012). WOOD DUST. In *www.ncbi.nlm.nih.gov*. International Agency for Research on Cancer. https://www.ncbi.nlm.nih.gov/books/NBK304376/#:~:text=Its%20composition%20varies%20considerably%20according

Ibrahim, J. E. F. M., Tihtih, M., & Gömze, L. A. (2021). Environmentally-friendly ceramic bricks made from zeolite-poor rock and sawdust. *Construction and Building Materials*, *297*, 123715. https://doi.org/10.1016/j.conbuildmat.2021.123715

Jannat, N., Latif Al-Mufti, R., Hussien, A., Abdullah, B., & Cotgrave, A. (2021). Influence of Sawdust Particle Sizes on the Physico-Mechanical Properties of Unfired Clay Blocks. *Designs*, *5*(3), 57. https://doi.org/10.3390/designs5030057

Johari, I., Said, S., Hisham, B., Bakar, A., & Ahmad, Z. A. (2010). Effect of the change of firing temperature on microstructure and physical properties of clay bricks from Beruas (Malaysia). *Science of Sintering*, *42*(2), 245–254. https://doi.org/10.2298/sos1002245j

Kotoyori, T. A. K. A. S. H. I. (1986). Critical ignition temperatures of wood sawdusts. *Fire Safety Science*, *1*, 463-471

Kornelia Wiśniewska, Waldemar Pichór, & Ewelina Kłosek-Wawrzyn. (2021). Influence of Firing Temperature on Phase Composition and Color Properties of Ceramic Tile Bodies. *Materials*, *14*(21), 6380–6380. https://doi.org/10.3390/ma14216380

Kristály, F., & Gömze, L. A. (2008). Remnants of organic pore-forming additives in conventional clay brickmaterials: Optical Microscopy and Scanning Electron

Microscopy study. *Epitoanyag - Journal of Silicate Based and Composite Materials*, *60*(2), 34–38. https://doi.org/10.14382/epitoanyag-jsbcm.2008.7

Kumar, S., Mote, V. D., Prakash, R., & Kumar, V. (2016). *X-ray Analysis of α-Al2O3 Particles by Williamson–Hall Methods*. *5*(6), 545–549. https://doi.org/10.1166/mat.2016.1345

Liu, J., Zhang, S. M., Chen, P. P., Cheng, L., Zhou, W., Tang, W. X., Chen, Z. W., & Ke, C. M. (2007). Controlled release of insulin from PLGA nanoparticles embedded within PVA hydrogels. *Journal of Materials Science: Materials in Medicine*, *18*(11), 2205–2210. https://doi.org/10.1007/s10856-007-3010-0

Liu, J., Ren, B., Lu, Y., Xi, X., Li, Y., Liu, K., Yang, J., & Huang, Y. (2019). *Novel design of elongated mullite reinforced highly porous alumina ceramics using carbonized rice husk as pore-forming agent*. *45*(11), 13964–13970. https://doi.org/10.1016/j.ceramint.2019.04.095

Luyten, J., Mullens, S., & Thijs, I. (2010). Designing with pores-synthesis and applications. *KONA Powder and Particle Journal*, *28*, 131-142.

Luz M.A. Maruoka, Pinheiro, I. F., Freitas, H. S., Francisco Xavier Nobre, & Vicente. (2023). Effect of thermal annealing on kaolin from the Amazon region, aiming at the production of geopolymer. *Journal of Materials Research and Technology*, *25*, 2471–2485. https://doi.org/10.1016/j.jmrt.2023.06.105

MANSARAY, K. G., & GHALY, A. E. (1997). Physical and Thermochemical Properties of Rice Husk. *Energy Sources*, *19*(9), 989–1004. https://doi.org/10.1080/00908319708908904

Mariscal-Becerra, L., Flores-Jiménez, M. C., Hernández-Álcantara, J. M., Camarillo, E., Falcony-Guajardo, C., Vázquez-Arreguín, R., & Murrieta Sanchez, H. (2018). Structural and luminescent analysis of hafnium-doped yttrium oxide and yttrium-doped

hafnium oxide powders and doped with trivalent europium and terbium ions. *Journal of Nanophotonics*, *12*(03), 1. https://doi.org/10.1117/1.jnp.12.036013

Martínez, J. R., Palomares-Sánchez, S., Ortega-Zarzosa, G., Ruiz, F., & Chumakov, Y. (2006). Rietveld refinement of amorphous SiO2 prepared via sol–gel method. *Materials Letters*, *60*(29-30), 3526–3529. https://doi.org/10.1016/j.matlet.2006.03.044

Matalkah, F., & Soroushian, P. (2018). Synthesis and characterization of alkali aluminosilicate hydraulic cement that meets standard requirements for general use. *Construction and Building Materials*, *158*, 42–49. https://doi.org/10.1016/j.conbuildmat.2017.10.002

Merga, A., Murthy, H. C. Ananda., Amare, E., Ahmed, K., & Bekele, E. (2019). Fabrication of electrical porcelain insulator from ceramic raw materials of Oromia region, Ethiopia. *Heliyon*, *5*(8), e02327. https://doi.org/10.1016/j.heliyon.2019.e02327

Narsinge, Ms. M. (2022). Study of Composite Bricks from Sawdust and Cement. *International Journal for Research in Applied Science and Engineering Technology*, *10*(5), 4978–4983. https://doi.org/10.22214/ijraset.2022.43523

Ngayakamo, B., & Park, E. (2019). Evaluation of Kalalani vermiculite for production of high strength porcelain insulators. *Science of Sintering*, *51*(2), 223–232. https://doi.org/10.2298/sos1902223n

Okunade, E. A. (2008). The Effect of Wood Ash and Sawdust Admixtures on the Engineering Properties of a Burnt Laterite-Clay Brick. *Journal of Applied Sciences*, *8*(6), 1042–1048. https://doi.org/10.3923/jas.2008.1042.1048

Olgun, A., Erdogan, Y., Ayhan, Y., & Zeybek, B. (2005). Development of ceramic tiles from coal fly ash and tincal ore waste. *Ceramics International*, *31*(1), 153–158. https://doi.org/10.1016/j.ceramint.2004.04.007

Pacheco-Torgal, F. (2015). Introduction to eco-efficient masonry bricks and blocks. In Eco-Efficient Masonry Bricks and Blocks (pp. 1-10). Woodhead Publishing.

Pedreño-Rojas, M. A., Morales-Conde, M. J., Rubio-de-Hita, P., & Pérez-Gálvez, F. (2019). Impact of Wetting–Drying Cycles on the Mechanical Properties and Microstructure of Wood Waste–Gypsum Composites. *Materials*, *12*(11), 1829. https://doi.org/10.3390/ma12111829

Phonphuak, N. (2020). The Use Of Sawdust Waste On Physical Properties And Thermal Conductivity Of Fired Clay Brick Production. *International Journal of GEOMATE*, *18*(69). https://doi.org/10.21660/2020.69.5706

Phonphuak, N., Kanyakam, S., & Chindaprasirt, P. (2016). Utilization of waste glass to enhance physical–mechanical properties of fired clay brick. *Journal of Cleaner Production*, *112*, 3057–3062. https://doi.org/10.1016/j.jclepro.2015.10.084

Progress in Biomass Conversion - 1st Edition. (n.d.). Shop.elsevier.com. Retrieved June 14, 2023, from https://shop.elsevier.com/books/progress-in-biomass-conversion/sarkanen/978-0-12-535903-0#:~:text=eBook%20ISBN%3A-

Ratnasinga, J., Natthondan, V., Ioras, F., & McNulty, T. (2010). Dust, Noise and Chemical Solvents Exposure of Workers in the Wooden Furniture Industry in South East Asia. *Journal of Applied Sciences*, *10*(14), 1413–1420. https://doi.org/10.3923/jas.2010.1413.1420

Ramamurthy, K., Nambiar, E. K., & Ranjani, G. I. S. (2009). A classification of studies on properties of foam concrete. Cement and concrete composites, 31(6), 388-396.

Rodríguez-Navarro, C., Cultrone, G., Navas, A., & Sebastián, E. (2003). TEM study of mullite growth after muscovite breakdown. *American Mineralogist*, *88*(5-6), 713–724. https://doi.org/10.2138/am-2003-5-601

S. Shoval, & Paz, Y. (2013). A study of the mass-gain of ancient pottery in relation to archeological ages using thermal analysis. *Applied Clay Science*, *82*, 113–120. https://doi.org/10.1016/j.clay.2013.06.027

Santa, A. C., Gómez, A., Castaño, J. G., Tamayo, J. A., & Baena, L. M. (2023). Atmospheric deterioration of ceramic building materials and future trends in the field: a review. *Heliyon*, *9*(4), e15028–e15028. https://doi.org/10.1016/j.heliyon.2023.e15028

SEDGHI, A., RIAHI-NOORI, N., HAMIDNEZHAD, N., & SALMANI, M. R. (2014). Effect of chemical composition and alumina content on structure and properties of ceramic insulators. *Bulletin of Materials Science*, *37*(2), 321–325. https://doi.org/10.1007/s12034-014-0641-x

Shafiquzzaman, Md., Alqarawi, S. M. A., Haider, H., Rafiquzzaman, Md., Almoshaogeh, M., Alharbi, F., & EL-Ghoul, Y. (2022). Sawdust Recycling in the Development of Permeable Clay Paving Bricks: Optimizing Mixing Ratio and Particle Size. *Sustainability*, *14*(18), 11115. https://doi.org/10.3390/su141811115

Shafizadeh, F. (1980). Alternative Energy Sources: *Progress in Biomass Conversion* . Vol. 1. Kyosti V. Sarkanen and David A. Tillman, Eds. Academic Press, New York, 1979. xii, 260 pp. $16.50.. *Science*, *209*(4459), 917–917. https://doi.org/10.1126/science.209.4459.917.a

Shrestha, D., Santi Maensiri, Unchista Wongpratat, Soo Wohn Lee, & Armila Rajbhandari Nyachhyon. (2019). Shorea robusta derived activated carbon decorated with manganese dioxide hybrid composite for improved capacitive behaviors. *Journal of Environmental Chemical Engineering*, *7*(5), 103227–103227. https://doi.org/10.1016/j.jece.2019.103227

Solongo, S., Franken, C., Tengis, S., Erdenebat Ulambayar, & Tumur-Ochir Batbayr. (2020). Multi-method (XRF, FTIR, TGA) analysis of ancient bricks from Karabalgasun

: A preliminary study. *Šinžlèh Uhaany Akademijn Mèdèè*. https://doi.org/10.5564/pmas.v60i1.1331

Sorna, S. M., Anjum, S. E., Ashraf, S. B., & Haque, R. (2016). Effects of Rice Husk Ash and Brick Waste on the Properties of Construction Bricks. *Applied Mechanics and Materials*, *860*, 81–86. https://doi.org/10.4028/www.scientific.net/amm.860.81

Sutcu, M., & Akkurt, S. (2009). The use of recycled paper processing residues in making porous brick with reduced thermal conductivity. Ceramics International, 35(7), 2625-2631.

Sylvain Meille, Lombardi, M., Chevalier, J., & Montanaro, L. (2012). *Mechanical properties of porous ceramics in compression: On the transition between elastic, brittle, and cellular behavior*. *32*(15), 3959–3967. https://doi.org/10.1016/j.jeurceramsoc.2012.05.006

Thalmaier, G., Cobîrzan, N., Balog, A. A., Constantinescu, H., Streza, M., Nasui, M., & Neamtu, B. V. (2020). Influence of sawdust particle size on fired clay brick properties. *Materiales de Construcción*, *70*(338), 215. https://doi.org/10.3989/mc.2020.04219

Uchechukwu Elinwa, A. (2006). Effect of addition of sawdust ash to clay bricks. *Civil Engineering and Environmental Systems*, *23*(4), 263–270. https://doi.org/10.1080/10286600600763149

Use of ceramics in construction. (n.d.). Www.designingbuildings.co.uk. https://www.designingbuildings.co.uk/wiki/Use_of_ceramics_in_construction

Vasconcelos da Silva, A. M., Delgado, J. M. P. Q., Guimarães, A. S., Barbosa de Lima, W. M. P., Soares Gomez, R., Pereira de Farias, R., Santana de Lima, E., & Barbosa de Lima, A. G. (2020). Industrial Ceramic Blocks for Buildings: Clay Characterization and Drying Experimental Study. *Energies*, *13*(11), 2834. https://doi.org/10.3390/en13112834

Wu, Z., Hu, W., Luo, Y., Sun, L., & Wang, J. (2018). Porous γ-(Y1-xHox) 2Si2O7 thermal insulator with excellent high-temperature strength retention and very low thermal conductivity. Journal of the European Ceramic Society, 38(9), 3347- 3353.

X-Ray Diffraction Analysis - an overview | ScienceDirect Topics. (n.d.). Www.sciencedirect.com. Retrieved June 30, 2023, from https://www.sciencedirect.com/topics/engineering/x-ray-diffraction-analysis

Xi, Y., Martens, W. N., He, H., & Frost, R. (2005). Thermogravimetric analysis of organoclays intercalated with the surfactant octadecyltrimethylammonium bromide. *Journal of Thermal Analysis and Calorimetry*, *81*(1), 91–97. https://doi.org/10.1007/s10973-005-0750-2

Yatim, N. H., & Rahman, H. A. (2020). Influences of Starch on Ceramic-Foam Fabrication: A Short Review. *IOP Conference Series: Materials Science and Engineering*, *824*(1), 012001. https://doi.org/10.1088/1757-899x/824/1/012001

Zakaria, S., Muhammad Zulkifli, Azhar, A., Budiman, F., Mohamed, Ali, A., Abdul Hafidz Yusoff, & Pao Ter Teo. (2020). Recycling of Wood Saw Dust Waste as Green Pore Forming Agent for Porous Ceramic. *IOP Conference Series*, *596*(1), 012017–012017. https://doi.org/10.1088/1755-1315/596/1/012017

Zhang, G., Xu, Y., Xu, D., Wang, D., Xue, Y., & Su, W. (2008). Pressure-induced crystallization of amorphous $SiO_2$with silicon–hydroxy group and the quick synthesis of coesite under lower temperature. *High Pressure Research*, *28*(4), 641–650. https://doi.org/10.1080/08957950802510091

Zhou, H., Qiao, X., & Yu, J. (2013). Influences of quartz and muscovite on the formation of mullite from kaolinite. *Applied Clay Science*, *80-81*, 176–181. https://doi.org/10.1016/j.clay.2013.04.004

APPENDIX A

Figure A1: The ceramic bricks dried in mould before firing for 2 days.

Figure A2: The ceramic bricks are set up for firing for 900 °C,1000 °C and 1100 °C.

.

Figure A3: The ceramic bricks after firing.

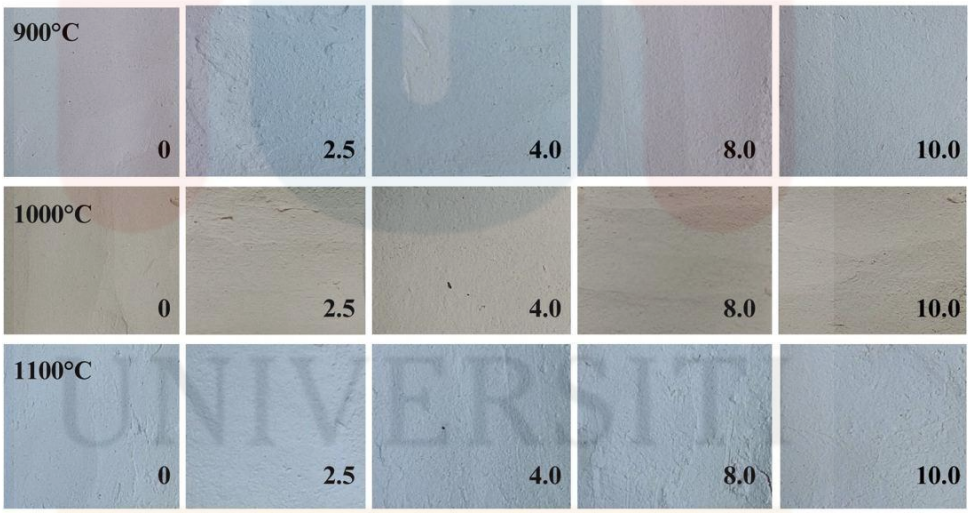

Figure A4: The structure of the ceramic brick of various composition after firing.

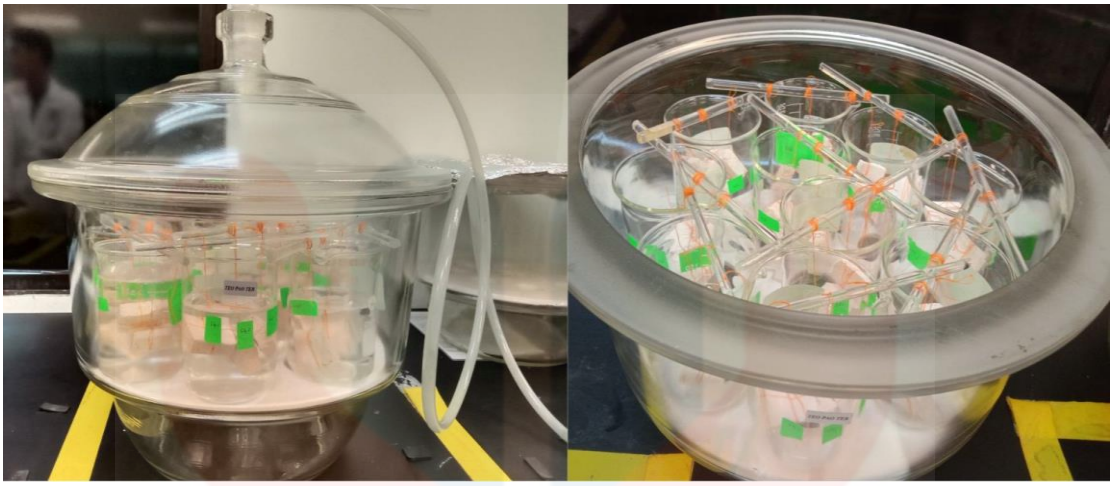

Figure A5: The characterization technique for density, water absorption and apparent porosity using densicator.

APPENDIX B

Pattern: COD 9009230 Radiation: 1.54060 Quality: Quality Unknown

Formula	Al2H4O9Si2
Name	
Name (mineral)	Kaolinite
Name (common)	
Status	Status Unknown
Ambient	Yes

Lattice:	Triclinic	Mol. weight =	
S.G.:	C 1 (1)	Volume [CD] =	329.89
		Dx =	
		Dm =	
		I/Icor =	1.220

a =	5.15540	alpha =	91.700
b =	8.94480	beta =	104.862
c =	7.40480	gamma =	89.822
a/b =	0.57636		
c/b =	0.82783		

Primary Reference
Bish D. L., Von Dreele R. B., "Rietveld refinement of non-hydrogen atomic positions in kaoliniteLocality: Keokuk, Iowa, USANote: clay", Clays and Clay Minerals 37 (1989) 289-296.

Wavelength:	1.54060	Filter:	Not specified
SS/FOM:		d-spacing:	

d	2θ	I fix	h	k	l	d	2θ	I fix	h	k	l
7.15390	12.363	999	0	0	1	2.18060	41.373	7	2	-2	0
4.47040	19.844	172	0	2	0	2.17200	41.544	6	2	2	0
4.36120	20.347	516	1	-1	0	2.15190	41.950	3	0	4	-1
4.34400	20.428	8	1	1	0	2.13060	42.390	21	0	-2	3
4.18090	21.234	494	1	1	-1	2.11560	42.705	8	0	4	1
4.12890	21.505	239	-1	1	1	2.09050	43.243	2	2	2	-2
3.84300	23.126	348	0	2	-1	2.07840	43.508	4	0	2	3
3.74120	23.764	146	0	2	1	2.06450	43.816	12	-2	2	2
3.57690	24.873	609	0	0	2	1.99760	45.364	81	-2	0	3
3.41850	26.045	16	1	-1	1	1.98590	45.646	76	1	-3	2
3.37370	26.397	192	1	1	1	1.97350	45.949	4	2	-2	1
3.15440	28.269	43	1	1	-2	1.95300	46.459	27	2	2	1
3.10360	28.742	47	-1	1	2	1.93880	46.820	56	1	3	2
2.83450	31.538	7	0	2	-2	1.92880	47.077	1	1	-1	3
2.75310	32.496	70	0	2	2	1.92150	47.267	27	0	4	-2
2.56620	34.936	63	2	0	-1	1.90750	47.635	6	1	1	3
2.56300	34.981	71	-1	3	0	1.89740	47.905	28	1	3	-3
2.55250	35.129	69	1	3	0	1.87060	48.635	25	0	4	2
2.53320	35.406	92	1	3	-1	1.84640	49.315	27	-1	3	3
2.51860	35.618	44	1	-1	2	1.83840	49.544	36	2	2	-3
2.49860	35.913	99	-1	3	1	1.83550	49.627	21	2	0	2
2.49140	36.020	99	2	0	0	1.81270	50.295	9	-1	-1	4
2.48600	36.101	24	1	1	2	1.80950	50.390	8	-2	2	3
2.38460	37.693	70	0	0	3	1.78850	51.023	32	0	0	4
2.34600	38.337	207	2	0	-2	1.70920	53.574	30	2	-2	2
2.33840	38.466	19	-1	-1	3	1.69040	54.219	17	2	4	-1
2.33530	38.519	193	-1	3	-1	1.68780	54.309	3	3	1	-1
2.30600	39.029	25	-1	1	3	1.68630	54.361	9	3	-1	-1
2.29280	39.262	248	1	3	1	1.68060	54.561	6	-2	4	1
2.25150	40.013	27	1	3	-2	1.68060	54.561	18	1	5	0
2.23520	40.317	2	0	4	0	1.67940	54.603	7	1	5	-1
2.21990	40.608	8	-2	2	1	1.67790	54.656	4	0	-2	4
2.19680	41.054	24	-1	3	2	1.66990	54.940	76	-2	0	4
2.18520	41.282	21	2	0	1	1.66760	55.022	33	-2	4	0

Pattern: COD 7105575 Radiation: 1.54060 Quality: Quality Unknown

Formula	Al4.8O9.6Si1.2
Name	
Name (mineral)	Mullite
Name (common)	
Status	Status Unknown
Ambient	Yes

Lattice:	Orthorhombic
S.G.:	P b a m (55)

a =	7.58800
b =	7.68800
c =	2.88950
a/b =	0.98699
c/b =	0.37585
Z =	1

Mol. weight =	
Volume [CD] =	168.56
Dx =	
Dm =	
I/Icor =	0.800

Primary Reference
Zhang Pengyu, Liu Jiachen, Du Haiyan, Li Sha, Xu Rui, "A facile preparation of mullite [Al(2)(Al(2.8)Si(1.2))O(9.6)]nanowires by B(2)O(3)-doped molten salts synthesis." (1991) 332-342.

Wavelength :	1.54060
SS/FOM:	
Filter:	Not specified
d-spacing:	

d	2θ	I fix	h	k	l	d	2θ	I fix	h	k	l
5.40050	16.401	742	1	1	0	1.46590	63.401	129	4	2	1
3.79400	23.429	14	2	0	0	1.44470	64.443	238	0	0	2
3.42910	25.963	571	1	2	0	1.42500	65.444	45	2	5	0
3.40230	26.171	999	2	1	0	1.41160	66.144	78	5	2	0
2.88950	30.922	209	0	0	1	1.39570	66.996	17	1	1	2
2.70030	33.149	490	2	2	0	1.35240	69.442	24	3	4	1
2.54780	35.196	524	1	1	1	1.35010	69.577	46	4	4	0
2.42790	36.996	151	1	3	0	1.33620	70.407	151	1	5	1
2.40260	37.400	12	3	1	0	1.33140	70.699	39	1	2	2
2.30970	38.963	3	0	2	1	1.32980	70.797	69	2	1	2
2.29870	39.158	241	2	0	1	1.32350	71.185	39	5	1	1
2.20960	40.805	623	1	2	1	1.31390	71.785	24	3	5	0
2.20240	40.945	37	2	1	1	1.30580	72.301	16	5	3	0
2.12360	42.536	261	2	3	0	1.28130	73.910	12	0	6	0
2.11300	42.760	33	3	2	0	1.27800	74.133	145	2	5	1
1.97290	45.964	6	2	2	1	1.27390	74.411	63	2	2	2
1.92200	47.254	16	0	4	0	1.26830	74.796	151	5	2	1
1.89700	47.915	73	4	0	0	1.26470	75.046	34	6	0	0
1.86320	48.841	18	1	4	0	1.26340	75.136	15	1	6	0
1.85880	48.964	2	1	3	1	1.24790	76.235	24	6	1	0
1.84740	49.286	120	3	1	1	1.24160	76.692	37	1	3	2
1.84180	49.446	14	4	1	0	1.23810	76.949	10	3	1	2
1.80020	50.668	11	3	3	0	1.22320	78.062	22	4	4	1
1.71450	53.396	67	2	4	0	1.21400	78.768	6	2	6	0
1.70560	53.697	99	3	2	1	1.20130	79.766	10	6	2	0
1.70110	53.850	116	4	2	0	1.19600	80.191	4	3	5	1
1.60030	57.547	178	0	4	1	1.19450	80.312	7	4	5	0
1.58580	58.123	62	4	0	1	1.19450	80.312	31	2	3	2
1.56590	58.934	11	1	4	1	1.19260	80.466	8	3	2	2
1.55310	59.468	10	4	1	1	1.18990	80.687	32	5	3	1
1.52790	60.551	470	3	3	1	1.15860	83.342	2	6	0	1
1.50700	61.481	7	1	5	0	1.15490	83.669	3	0	4	2
1.48890	62.311	4	5	1	0	1.14940	84.161	13	4	0	2
1.47450	62.989	11	2	4	1	1.14170	84.861	2	1	4	2

Pattern: COD 1011172 Radiation: 1.54060 Quality: Quality Unknown

Formula	O2Si
Name	
Name (mineral)	Quartz low
Name (common)	
Status	Status Unknown
Ambient	Yes

Lattice:	Hexagonal
S.G.:	P 31 2 1 (152)

a =	4.91300
c =	5.40500
a/b =	1.00000
c/b =	1.10014
Z =	3

Mol. weight =	
Volume [CD] =	112.98
Dx =	
Dm =	
I/Icor =	3.280

Primary Reference
Brill R, Hermann C, Peters C, "Studien ueber chemische Bindung mittels Fourieranalyse III. Die Bindungim Quarz", Naturwissenschaften 27 (1939) 676-677.

Wavelength :	1.54060
SS/FOM:	
Filter:	Not specified
d-spacing:	

d	2θ	I fix	h	k	l
4.25480	20.861	204	1	0	0
3.34320	26.642	1000	1	0	1
2.45650	36.550	72	1	1	0
2.28120	39.470	73	1	0	2
2.23640	40.295	35	1	1	1
2.12740	42.457	52	2	0	0
1.97960	45.799	30	2	0	1
1.81780	50.144	117	1	1	2
1.80170	50.623	2	0	0	3
1.67160	54.880	45	2	0	2
1.65910	55.328	15	1	0	3
1.60820	57.238	3	2	1	0
1.54140	59.966	84	2	1	1
1.45280	64.040	20	1	1	3
1.41830	65.792	3	3	0	0
1.38200	67.750	52	2	1	2
1.37490	68.147	60	2	0	3
1.37180	68.323	43	3	0	1
1.28790	73.469	20	1	0	4
1.25580	75.671	24	3	0	2
1.22830	77.677	11	2	2	0
1.19970	79.894	29	2	1	3
1.19770	80.054	9	2	2	1
1.18400	81.172	23	1	1	4
1.18010	81.497	28	3	1	0
1.15290	83.848	13	3	1	1
1.14060	84.962	3	2	0	4
1.11440	87.454	2	3	0	3
1.08150	90.837	27	3	1	2
1.06370	92.800	3	4	0	0
1.04770	94.653	14	1	0	5
1.04370	95.131	11	4	0	1
1.03450	96.251	14	2	1	4
1.01490	98.751	11	2	2	3

Pattern: COD 1100013 Radiation: 1.54060 Quality: Quality Unknown

Formula	Al3HKO12Si3
Name	
Name (mineral)	Muscovite 2M1
Name (common)	
Status	Status Unknown
Ambient	Yes

Lattice:	Monoclinic
S.G.:	C 1 2/c 1 (15)

Mol. weight =	
Volume [CD] =	932.03
Dx =	
Dm =	
I/Icor =	3.200

a =	5.18000	**beta =**	95.500
b =	9.02000		
c =	20.04000	**Z =**	4
a/b =	0.57428		
c/b =	2.22173		

Primary Reference
Jackson W W, West J, Zeitschrift fuer Kristallographie, Kristallgeometrie, Kristallphysik,Kristallchemie (-144,1977) 76 (1931) 211-227.

Wavelength :	1.54060
SS/FOM:	
Filter:	Not specified
d-spacing:	

d	2θ	I f|x	h	k	l
9.97390	8.859	103	0	0	2
4.98690	17.772	62	0	0	4
4.47640	19.818	51	1	1	0
4.39900	20.170	16	0	2	1
4.29210	20.678	1000	1	1	1
4.21710	21.050	10	-1	1	2
4.10940	21.608	10	0	2	2
3.88530	22.990	285	-1	1	3
3.73240	23.821	69	0	2	3
3.57800	24.865	33	1	1	3
3.47820	25.590	149	-1	1	4
3.34500	26.628	101	0	2	4
3.32460	26.794	75	0	0	6
3.20140	27.846	122	1	1	4
3.10960	28.685	6	-1	1	5
2.98820	29.877	26	0	2	5
2.86240	31.223	27	1	1	5
2.78210	32.148	40	-1	1	6
2.67610	33.458	2	0	2	6
2.59170	34.581	13	-1	3	1
2.57810	34.769	52	2	0	0
2.56870	34.901	48	1	1	6
2.55980	35.026	50	1	3	1
2.55610	35.078	12	2	0	-2
2.50000	35.892	32	-1	1	7
2.49350	35.989	11	0	0	8
2.45990	36.497	27	-1	3	3
2.44000	36.806	48	2	0	2
2.38530	37.681	3	-2	0	4
2.38070	37.757	8	1	3	3
2.31810	38.817	8	1	1	7
2.25500	39.948	8	0	4	0
2.24500	40.134	7	2	2	-1
2.24070	40.214	2	0	4	1
2.22640	40.484	8	-1	3	5
2.22380	40.533	29	2	2	-2
2.20550	40.885	33	2	0	4
2.18220	41.341	3	0	2	8
2.17870	41.450	24	-2	2	3
2.14810	42.069	6	2	2	2
2.13900	42.215	18	-2	0	6
2.13550	42.288	12	0	4	3
2.13020	42.398	76	1	3	5
2.06980	43.698	4	2	2	3
2.05540	44.020	63	-1	1	9
2.05470	44.036	6	0	4	4
2.02520	44.712	6	-2	2	5
1.99480	45.431	51	0	0	10
1.98130	45.758	1	2	2	4
1.96750	46.097	22	-1	3	7
1.96310	46.207	7	0	4	5
1.94890	46.563	21	2	0	6
1.92360	47.212	6	1	1	9
1.88820	48.207	7	2	2	5
1.88490	48.242	7	-2	0	8
1.86620	48.757	3	0	4	6
1.83900	49.613	1	-2	2	7
1.82430	49.953	2	0	2	10
1.78900	51.008	1	2	2	6
1.73910	52.582	6	-2	2	8
1.73160	52.827	4	-1	1	11
1.70280	53.792	2	1	5	0
1.70120	53.847	3	-1	5	1
1.70030	53.877	2	2	4	-1
1.69730	53.980	4	2	4	0
1.69210	54.160	21	1	5	1
1.69110	54.195	2	3	1	-2
1.69100	54.198	3	-2	4	2

d	2θ	I f/c	h	k	l	d	2θ	I f/c	h	k	l	d	2θ	I f/c	h	k	l
1.68830	54.292	1	3	1	0	1.49010	62.255	28	-1	1	13	1.28600	73.595	1	3	1	9
1.68250	54.494	5	0	2	11	1.48850	62.423	5	0	6	2	1.28020	73.984	3	-2	4	11
1.67450	54.777	2	3	1	-3	1.48250	62.610	1	-1	5	7	1.27990	74.004	13	2	6	2
1.67000	54.937	9	-2	4	3	1.47450	62.989	5	2	4	6	1.27890	74.072	7	3	3	7
1.66920	54.965	10	3	1	1	1.47010	63.199	5	-2	2	11	1.27810	74.126	1	4	0	-4
1.66230	55.213	2	0	0	12	1.46240	63.570	22	-2	0	12	1.27180	74.555	4	-2	6	4
1.65640	55.426	23	-2	0	10	1.45270	64.045	8	0	2	13	1.26860	74.775	5	0	4	13
1.65610	55.437	1	2	4	2	1.45120	64.119	7	3	1	6	1.26310	75.157	3	4	0	2
1.64720	55.763	7	1	3	9	1.43740	64.810	12	-3	3	5	1.25000	76.084	3	-2	2	14
1.64700	55.770	9	-3	1	4	1.43120	65.125	2	2	2	10	1.24670	76.322	6	6	0	16
1.63720	56.133	28	1	5	3	1.43070	65.151	5	3	3	3	1.24590	76.380	6	1	7	1
1.63410	56.249	1	1	1	11	1.42480	65.454	4	0	0	14	1.24460	76.474	2	-3	1	12
1.62730	56.505	11	-1	5	4	1.41580	65.923	3	1	1	13	1.24410	76.510	1	4	2	-1
1.62030	56.772	1	2	4	3	1.41320	66.060	3	0	4	11	1.24270	76.612	2	-4	0	6
1.61020	57.160	8	-3	1	5	1.40850	66.308	9	-3	1	9	1.24220	76.648	19	2	6	4
1.60250	57.460	3	-1	1	12	1.39600	66.980	6	3	1	7	1.23920	76.868	4	4	2	-3
1.60090	57.523	1	3	1	3	1.39160	67.220	2	-1	1	14	1.23880	76.897	7	-3	5	3
1.60070	57.531	1	2	2	8	1.39110	67.247	2	-2	2	12	1.23660	77.059	10	3	5	1
1.59860	57.614	3	-2	4	5	1.37140	68.345	1	-1	5	9	1.22960	77.579	2	4	2	-4
1.59610	57.713	10	1	5	4	1.35000	69.583	2	-1	3	13	1.22750	77.737	3	-3	5	4
1.58610	58.926	2	-3	1	6	1.33980	70.190	1	2	0	12	1.22340	78.047	7	1	7	3
1.55970	59.191	3	0	2	12	1.33800	70.299	6	0	4	12	1.22000	78.306	2	4	0	4
1.55530	59.376	8	3	1	4	1.33010	70.779	13	1	5	9	1.21930	78.360	3	-1	7	4
1.55480	59.397	3	-2	2	10	1.32620	71.018	3	1	1	14	1.21920	78.367	3	2	2	13
1.55190	59.519	4	-2	4	6	1.31780	71.540	5	-2	2	13	1.20880	79.173	1	-1	5	12
1.53540	60.224	4	-1	5	6	1.30480	72.365	2	-1	1	15	1.20810	79.228	1	3	5	3
1.52750	60.568	3	2	4	5	1.30100	72.610	1	-2	0	14	1.20760	79.267	5	-1	3	15
1.52180	60.819	6	-1	3	11	1.29870	72.759	23	2	6	0	1.20600	79.393	3	1	7	4
1.51770	61.001	2	1	1	12	1.29820	72.792	8	-3	1	11	1.20060	79.822	4	0	6	10
1.50920	61.381	19	2	0	10	1.29430	73.046	2	4	0	-2	1.19930	79.926	1	2	0	14
1.50480	61.580	5	3	1	5	1.29400	73.066	1	1	3	13	1.19270	80.458	5	-4	0	8
1.50330	61.648	32	0	6	0	1.28900	73.396	14	4	0	0	1.19270	80.458	1	3	3	9
1.49730	61.923	2	3	3	-1	1.28840	73.435	7	-3	3	9						
1.49650	61.959	6	1	5	6	1.28740	73.502	9	0	6	8						

APPENDIX C

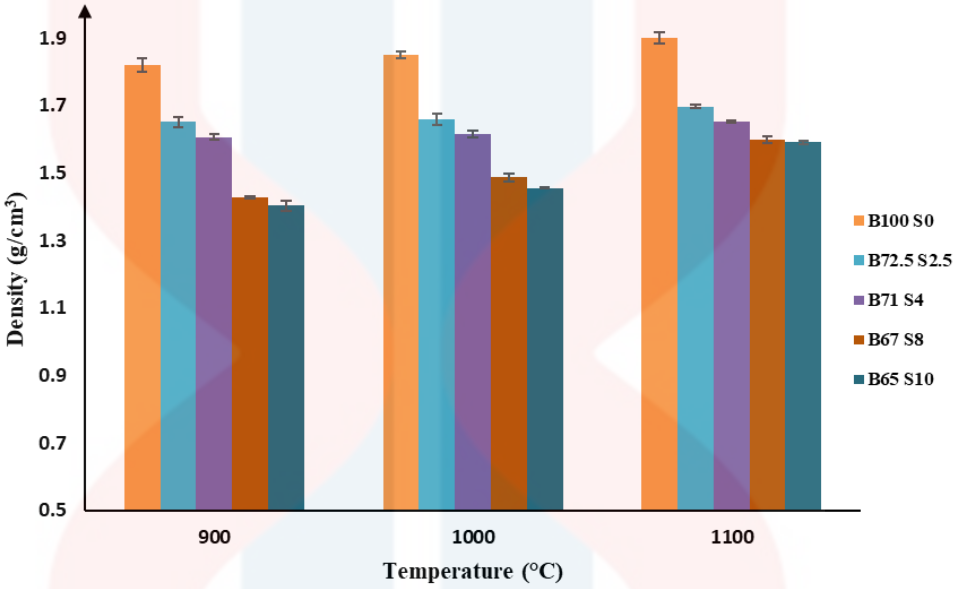

Figure C1: Density value for various sample fired at 900 °C,1000 °C and 1100 °C.

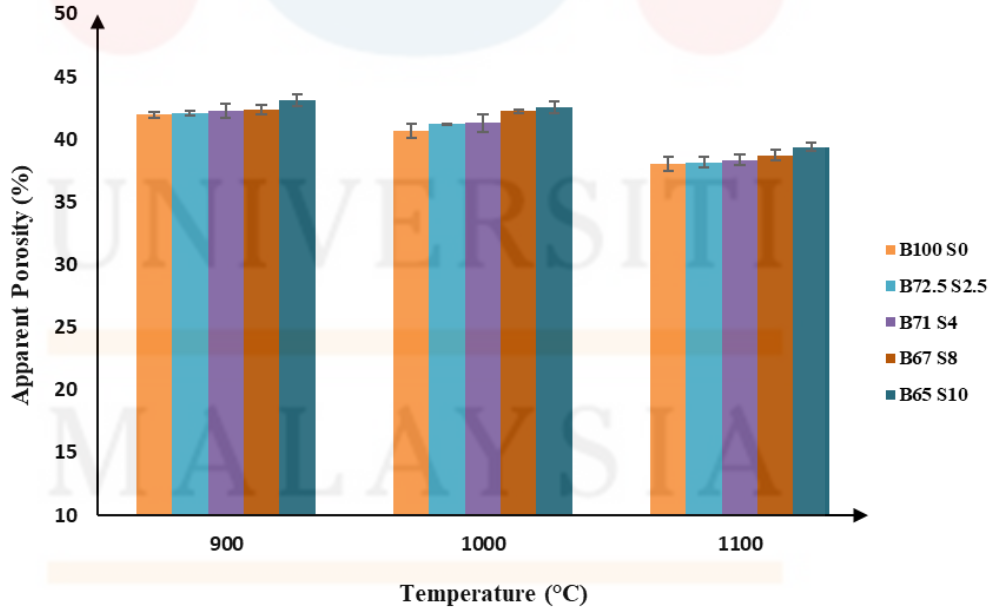

Figure C2: Apparent porosity for various sample fired at 900 °C,1000 °C and 1100 °C.

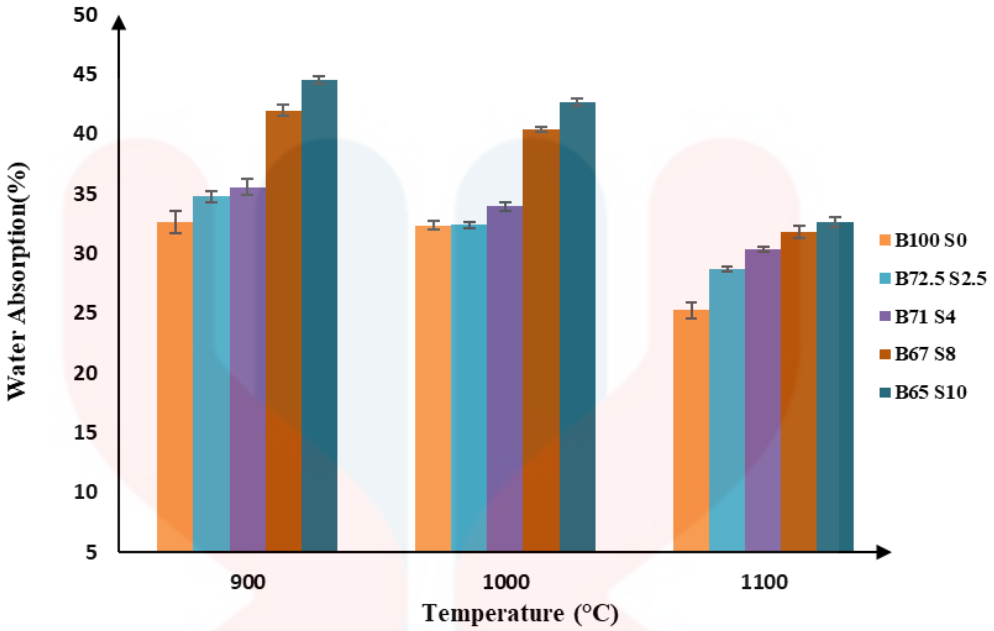

Figure C3: Water absorption for various sample fired at 900 °C,1000 °C and 1100 °C.

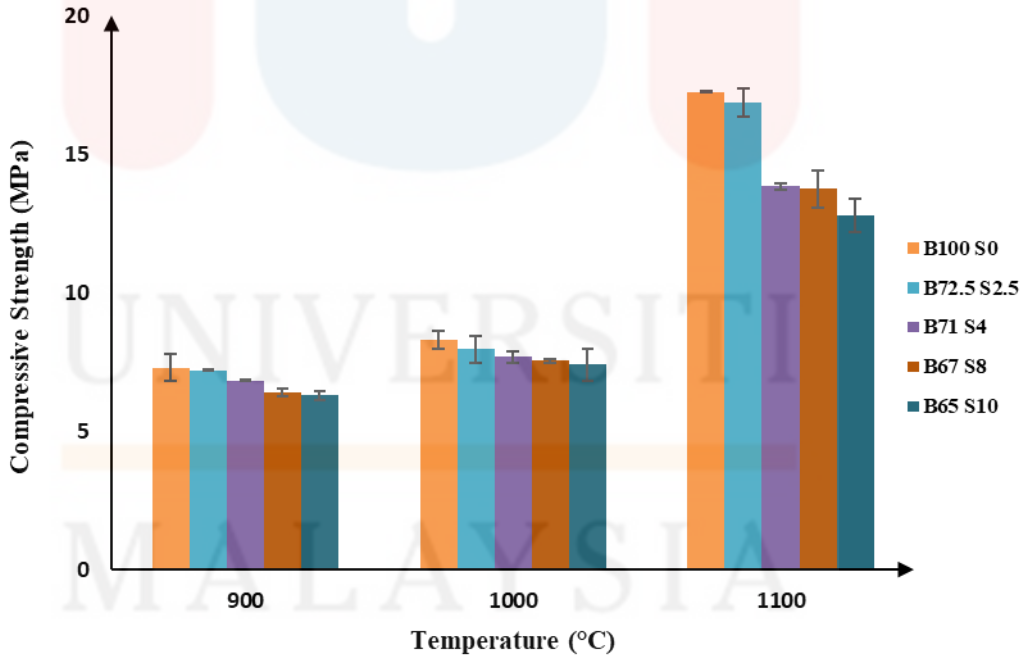

Figure C4: Compressive strength for various sample fired at 900 °C,1000 °C and 1100 °C.